

Ubiquitination-dependent quality control of hERG K⁺ channel with acquired and inherited conformational defect at the plasma membrane

Pirjo M. Apaja, Brian Foo, Tsukasa Okiyoneda, William C. Valinsky, Herve Barriere, Roxana Atanasiu, Eckhard Ficker, Gergely L. Lukacs, and Alvin Shrier

Department of Physiology and Groupe de Recherche Axé sur la Structure des Protéines, McGill University, Montréal, QC H3E 1Y6, Canada

ABSTRACT Membrane trafficking in concert with the peripheral quality control machinery plays a critical role in preserving plasma membrane (PM) protein homeostasis. Unfortunately, the peripheral quality control may also dispose of partially or transiently unfolded polypeptides and thereby contribute to the loss-of-expression phenotype of conformational diseases. Defective functional PM expression of the human ether-a-go-go-related gene (hERG) K⁺ channel leads to the prolongation of the ventricular action potential that causes long QT syndrome 2 (LQT2), with increased propensity for arrhythmia and sudden cardiac arrest. LQT2 syndrome is attributed to channel biosynthetic processing defects due to mutation, drug-induced misfolding, or direct channel blockade. Here we provide evidence that a peripheral quality control mechanism can contribute to development of the LQT2 syndrome. We show that PM hERG structural and metabolic stability is compromised by the reduction of extracellular or intracellular K⁺ concentration. Cardiac glycoside-induced intracellular K⁺ depletion conformationally impairs the complex-glycosylated channel, which provokes chaperone- and C-terminal Hsp70-interacting protein-dependent polyubiquitination, accelerated internalization, and endosomal sorting complex required for transport-dependent lysosomal degradation. A similar mechanism contributes to the down-regulation of PM hERG harboring LQT2 missense mutations, with incomplete secretion defect. These results suggest that PM quality control plays a determining role in the loss-of-expression phenotype of hERG in certain hereditary and acquired LQT2 syndromes.

Monitoring Editor

Thomas Sommer
Max Delbrück Center for Molecular Medicine

Received: Jul 25, 2013

Revised: Oct 7, 2013

Accepted: Oct 17, 2013

INTRODUCTION

The human ether-a-go-go-related gene (hERG) encodes the α subunit of the Kv11.1 channel, which is responsible for the rapidly

This article was published online ahead of print in MBoC in Press (<http://www.molbiolcell.org/cgi/doi/10.1091/mbc.E13-07-0417>) on October 23, 2013.

Address correspondence to: A. Shrier (alvin.shrier@mcgill.ca), G. L. Lukacs (gergely.lukacs@mcgill.ca).

Abbreviations used: Ab, antibody; Baf, bafylomycin A1; CHIP, C-terminal Hsp70-interacting protein; cs-ELISA, cell-surface enzyme-linked immunosorbent assay; ESCRT, endosomal sorting complex required for transport; FITC, fluorescein isothiocyanate; FRIA, fluorescence ratio image analysis; MVB, multivesicular body; Nedd4-2, neural precursor cell expressed developmentally down-regulated protein 4 long isoform; NT, nontargeted; pH_v, vesicular pH; PM, plasma membrane; QC, quality control; SF, selectivity filter; Ub, ubiquitin; wt, wild type.

© 2013 Apaja et al. This article is distributed by The American Society for Cell Biology under license from the author(s). Two months after publication it is available to the public under an Attribution–Noncommercial–Share Alike 3.0 Unported Creative Commons License (<http://creativecommons.org/licenses/by-nc-sa/3.0/>).

“ASCB®,” “The American Society for Cell Biology®,” and “Molecular Biology of the Cell®” are registered trademarks of The American Society of Cell Biology.

activating delayed rectifier potassium current (I_{Kr}). The I_{Kr} plays a key role in the terminal phase of the repolarization of the cardiac ventricular action potential (Sanguinetti et al., 1995). Reduction of hERG function delays ventricular repolarization and increases the duration of the cardiac action potential. The consequence is a prolongation of the QT interval on the electrocardiogram and associated long QT type 2 (LQT2) syndrome, which increases the propensity for torsades de pointes arrhythmia and sudden cardiac arrest (Keating and Sanguinetti, 2001; Sanguinetti and Tristani-Firouzi, 2006). Inherited LQT2 is caused by mutations in the hERG gene, whereas the acquired form of LQT2 is the result of off-target drug effects.

The hERG K⁺ channel is a tetrameric complex, with each subunit consisting of a cytoplasmic N-terminal (Per-Arnt-Sim [PAS]), a C-terminal (cyclic nucleotide homology binding) domain, and a transmembrane region that forms the voltage sensor and ion-conducting pore, including the selectivity filter (Vandenberg et al., 2012). Channel

biosynthetic maturation, which is assisted by molecular chaperones (e.g., Hsp70/Hsc70, DJA1, DJA2, and Hsp90), can be compromised to variable extents by several LQT2-associated missense mutations (Ficker et al., 2003; Anderson et al., 2006; Walker et al., 2010). Mutations within the PAS domain can cause partial processing defects and reach the plasma membrane (PM); these are metabolically unstable by an unknown mechanism (Ke et al., 2013).

Drug-induced LQT2 is frequently caused by impaired biosynthesis and/or functional blockade of hERG (Ficker et al., 2004; Kuryshov et al., 2005) and can be provoked by many compounds, including arsenic trioxide (Ficker et al., 2004), the antiprotozoal agent pentamidine (Cordes et al., 2005; Kuryshov et al., 2005), the cholesterol-lowering compound probucol (Guo et al., 2007), the antidepressant fluoxetine (Prozac), and the antifungal drug ketoconazole (Wible et al., 2005; Rajamani et al., 2006; Takemasa et al., 2008). Cardiac glycosides, a family of Na^+/K^+ -ATPase inhibitors commonly used in the treatment of congestive heart failure and cardiac arrhythmia, have been shown to decrease cytoplasmic $[\text{K}^+]$ ($[\text{K}^+]_{\text{cy}}$), which compromises hERG conformational maturation at the ER without influencing its tetramerization (Hauptman and Kelly, 1999; Gheorghiade and Lukas, 2004; Wang et al., 2007). Of note, reducing the extracellular K^+ concentration ($[\text{K}^+]_{\text{ex}}$) provokes the accelerated internalization and lysosomal degradation of wild-type (wt) hERG (Guo et al., 2009), which is attributed to hERG monoubiquitination at the PM (Guo et al., 2009; Sun et al., 2011).

Structural destabilization of PM proteins can signal their removal in both yeast and higher eukaryotes. According to prevailing models, a network of molecular chaperones or adaptor proteins can recognize the conformational defect and mediate the recruitment of a subset of E3 ubiquitin ligases (e.g., Rsp5 and C-terminal Hsp70-interacting protein [CHIP]; Okiyone et al., 2011; MacGurn et al., 2012; Keener and Babst, 2013). Subsequent polyubiquitination or multiple monoubiquitination by the peripheral quality control (QC) machinery serves as efficient internalization and lysosomal sorting signal for the handful of physiological substrates (e.g., mutant cystic fibrosis transmembrane conductance regulator [CFTR] and G-protein coupled receptors [GPCR]), which can either constitutively or after rescue reach the PM in higher eukaryotes (Apaja et al., 2010; Okiyone et al., 2010; MacGurn et al., 2012).

In the present study we test whether conformational destabilization of hERG by cytosolic or extracellular K^+ depletion or genetic mutations can serve as a signal for recognition and accelerated degradation by the peripheral QC. We demonstrate that both K^+ depletion and selected LQT2 associated mutations compromise hERG structural stability at the PM. This in turn results in polyubiquitination and multiple monoubiquitination of hERG by a CHIP-dependent mechanism, which leads to metabolic destabilization via accelerated internalization and endosomal sorting complex required for transport (ESCRT)-dependent lysosomal degradation. These results identify hERG with either an acquired or inherited conformational defect as a previously unrecognized substrate for the peripheral QC machinery, contributing to the pathogenesis of the LQT2 syndrome.

RESULTS

Cardiac glycosides destabilize the hERG channel at the plasma membrane

Cardiac glycoside-induced acquired LQT2 has been attributed to a biosynthetic maturation defect of newly translated hERG at the endoplasmic reticulum (ER) ostensibly due to $[\text{K}^+]_{\text{cy}}$ depletion (Wang et al., 2007). On the basis of sequence conservation between hERG

and KcsA selectivity filter (SF), the collapsed SF crystal structure of KcsA in low K^+ , and enthalpic stabilization of KcsA by K^+ (Zhou and MacKinnon, 2003; Krishnan et al., 2005; Lockless et al., 2007), we postulated that K^+ ions may be critical in the structural and metabolic stabilization of the mature hERG in post-ER compartments, including the PM.

HeLa cells heterologously expressing hERG channels bearing a hemagglutinin (HA) tag in the first extracellular loop (S1–S2; Ficker et al., 2003) were exposed to cardiac glycosides (ouabain, digoxin, or digitoxin) at therapeutic plasma concentration (5–20 nM) for 24 h (Beller et al., 1971). Glycoside treatment at concentrations >15 nM decreased the mature, complex-glycosylated (Figure 1, A and B) and PM-resident hERG pools (Figure 1C) >50% as determined by immunoblotting and cell-surface enzyme-linked immunosorbent assay (ELISA), respectively. The steady-state reduction of the PM hERG density can be at least partly attributed to the accelerated channel turnover, as measured by PM ELISA after 24 h of glycoside treatment (Figure 1D). Cell-surface hERG was detected by anti-HA antibody (Ab) and horseradish peroxidase (HRP)-conjugated secondary Ab in the presence of Amplex Red. Thus therapeutic doses of glycosides may contribute to down-regulation of hERG by accelerating the channel turnover at the PM. Atomic adsorption spectroscopy measurements showed that treatment of HeLa cells with 10 nM ouabain, digoxin, or digitoxin for 24 h led to 50, 45, and 60% loss of $[\text{K}^+]_{\text{cy}}$, respectively (Figure 1E, left).

To model the consequence of therapeutic doses of glycosides on cellular K^+ loss and hERG trafficking, we exposed cells to pharmacological doses of glycosides. Exposure to 300 nM ouabain reduced $[\text{K}^+]_{\text{cy}}$ by 50% after 1 h and 90% after 3 h (Figure 1E, right) as a result of Na^+/K^+ -ATPase inhibition and depolarization-induced K^+ efflux. Cell viability remained >80% during both acute and long-term glycoside treatment (Supplemental Figure S1A and unpublished data). In contrast to the glycoside effect, extracellular hypokalemia (0.1 mM $[\text{K}^+]_{\text{ex}}$) led to a loss of $[\text{K}^+]_{\text{cy}}$ that was three times slower (Figure 1E, right).

Ouabain or digoxin (300 nM) profoundly accelerated the disappearance of complex-glycosylated hERG (~155 kDa), with a half-life ($t_{1/2}$) of ~3 h, in contrast to the slow diminution induced by the translational inhibitor cycloheximide (Figure 1, F and G). Similar results were obtained in H9C2_i rat cardiac myocytes heterologously expressing hERG under the control of a tetracycline-inducible transactivator (Figure 1F). These observations support the notion that glycoside-induced down-regulation of PM hERG contributes to the expression defect in post-ER compartments, an inference confirmed by the following observations. 1) The rapid PM removal of hERG was confirmed by indirect immunostaining and cell surface biotinylation in conjunction with immunoblotting (Figure 2, A and B). 2) The PM turnover of hERG was accelerated threefold upon ouabain or digoxin treatment in HeLa ($t_{1/2} \approx 3$ h) and H9C2_i ($t_{1/2} \approx 1$ h) cells as compared with untreated cells ($t_{1/2} \approx 9$ and 3 h, respectively; Figure 2C). 3) Neither the stability (Figure 2D) nor the cellular or cell surface expression of other PM proteins (CFTR, Sharma et al., 2004; megalencephalic leukoencephalopathy with subcortical cysts 1 [MLC1], Duarri et al., 2008; vasopressin 2 receptor [V2R] and dopamine D4 receptor [DRD4], Apaja et al., 2010) was influenced by ouabain (Figure 2D and Supplemental Figure S1, B and C). 4) Mutations at or near the SF (e.g., F627Y and S641A) that conferred partial resistance to the cardiac glycoside-induced ER processing defect of hERG (Wang et al., 2009) also desensitized hERG at the PM. Whereas F627Y and S641A decreased steady-state PM hERG expression

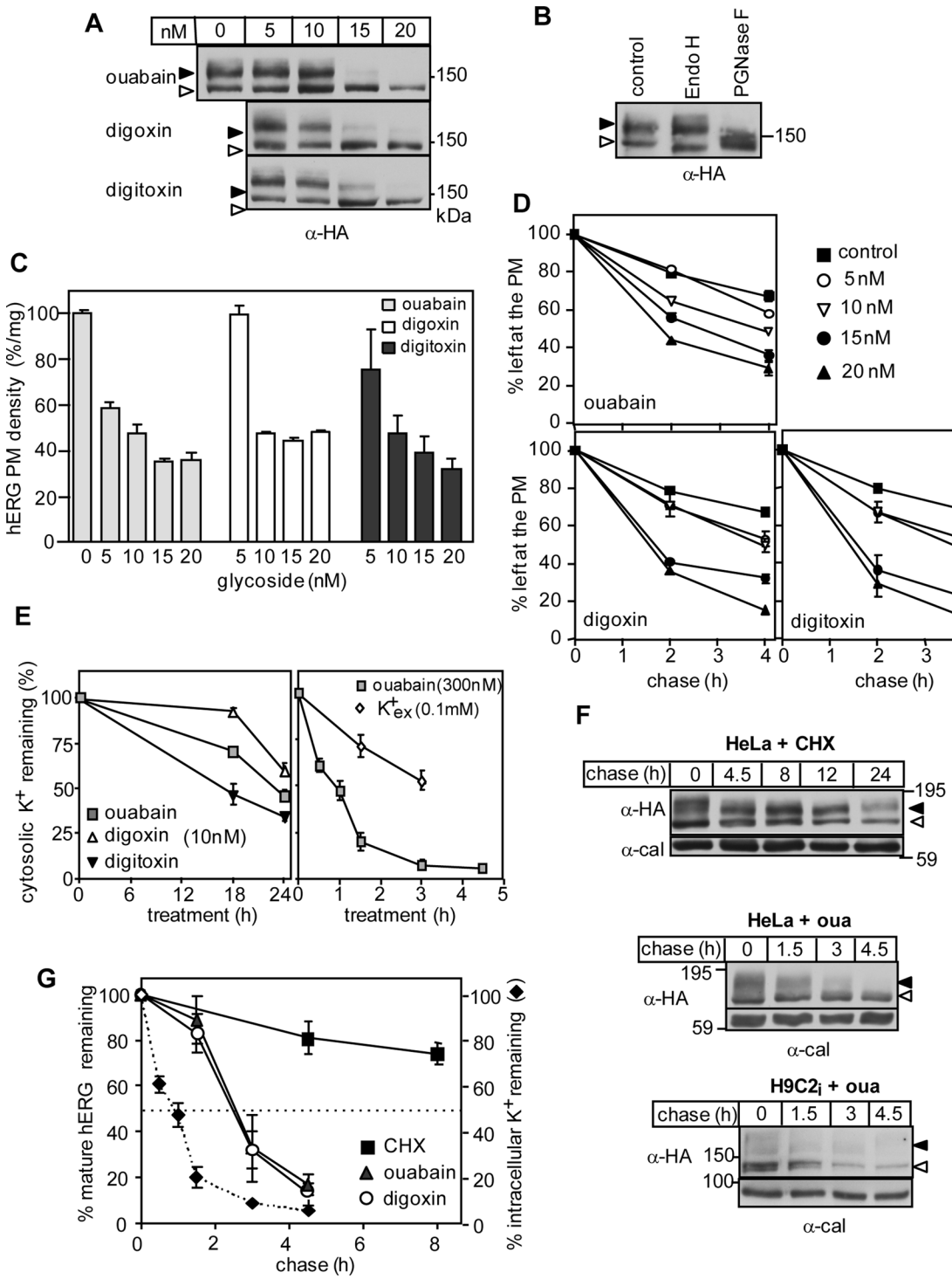


FIGURE 1: Intracellular potassium depletion decreases mature hERG half-life. (A) HeLa cells expressing hERG were treated for 24 h with cardiac glycosides and analyzed by immunoblotting for total hERG expression. Solid arrow, complex-glycosylated hERG; empty arrow, core-glycosylated hERG. (B) Glycosylation state of wt hERG in HeLa cell lysate after EndoH or PNGaseF digestion (3 h at 30°C) assessed with immunoblotting. (C, D) PM density and turnover of hERG determined by cell-surface (cs)-ELISA after 24-h treatment with the indicated glycoside. Data are expressed as percentage of initial hERG density. Data are means \pm SEM, $n \geq 3$ independent experiments, each performed in triplicate. (E) Intracellular K⁺ content of wt hERG-expressing HeLa cells after incubation with ouabain or K⁺-free (0.1 mM K⁺) media measured with flame emission spectroscopy. (F) Turnover of hERG in HeLa cells (top and middle) and H9C2_i cardiac myocytes (bottom) in the presence of 150 μ g/ml cycloheximide or 300 μ M ouabain as indicated. Calnexin (cal) was used as loading control. (G) Densitometry of complex-glycosylated hERG turnover based on immunoblots as shown in F. The reduction of intracellular K⁺ content is also plotted during 300 nM ouabain exposure. dig, digoxin; oua, ouabain.

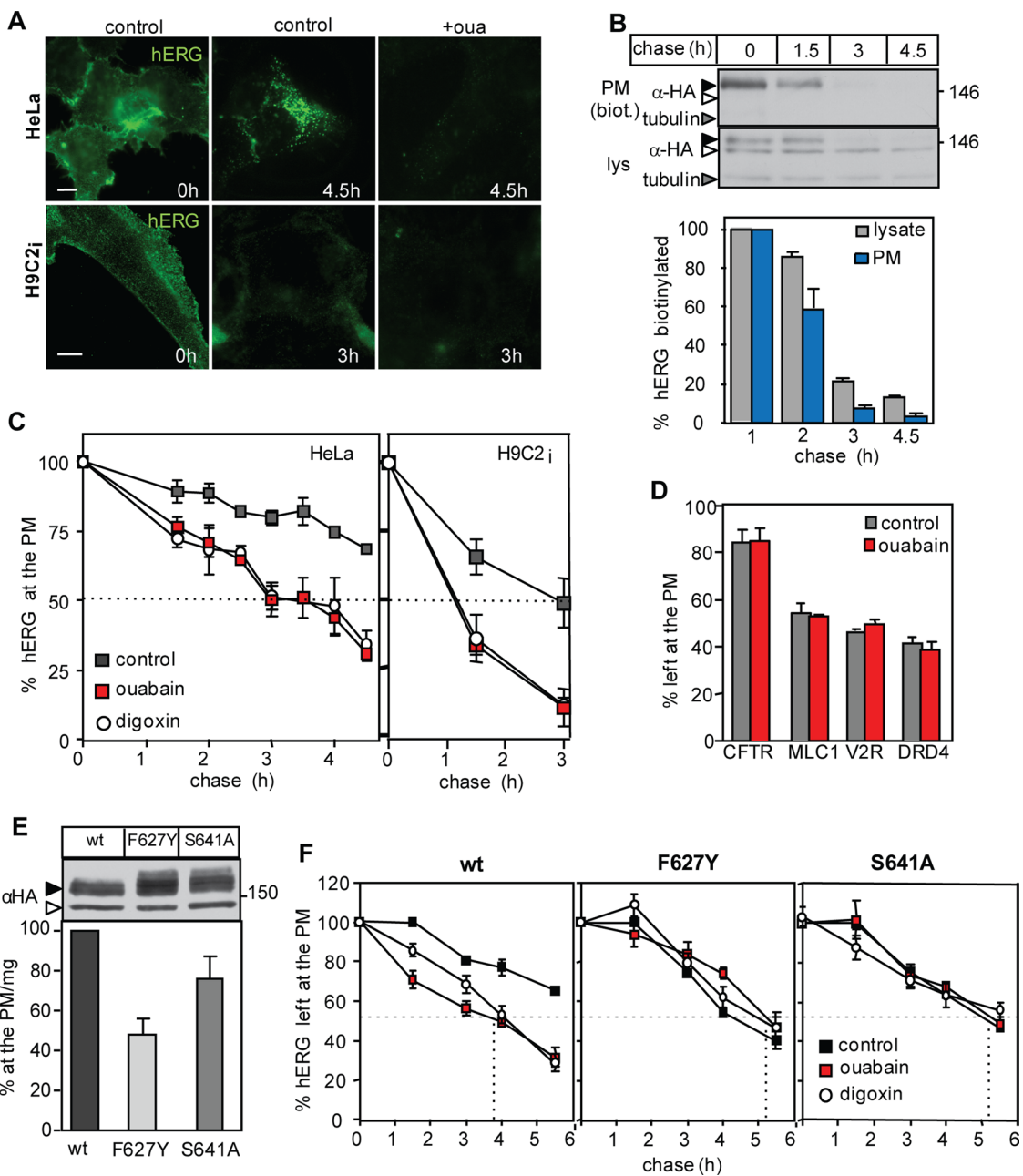


FIGURE 2: Intracellular potassium depletion destabilizes hERG channels at the plasma membrane. (A) Indirect immunostaining of PM hERG in ouabain-treated HeLa (top; bar, 10 μ m) and H9C2_i cells (bottom; bar, 15 μ m) by epifluorescence microscopy. Cell-surface hERG was labeled with anti-HA Ab on ice and chased for 0, 3, or 4.5 h at 37°C, fixed, and stained without permeabilization. (B) Cell-surface proteins were labeled with sulfo-NHS-SS-biotin after the indicated ouabain treatment and isolated on NeutrAvidin-agarose beads. Biotinylated hERG was detected using anti-HA Ab. Neither the core-glycosylated, ER-resident hERG nor tubulin was accessible to biotinylation. Bottom, densitometric analysis of biotinylated and total hERG pool turnover. Data are means \pm SEM, $n \geq 3$. (C) PM turnover of hERG in HeLa (left) and H9C2_i (right) cells determined by cs-ELISA in the presence of 300 nM glycosides. (D) Stability of CFTR, MLC1, V2R, and DRD4.4 determined by cs-ELISA after 3.5 h 300 nM ouabain treatment. (E) Cellular and PM expression of wt, F627Y, and S641A hERG measured by immunoblotting and cs-ELISA. (F) PM stability of wt, S627Y, and S641A hERG determined by cs-ELISA. Dashed line, $t_{1/2}$ of PM hERG stability in ouabain-treated HeLa cells. dig, digoxin; oua, ouabain. Data are means \pm SEM, $n = 3$.

(Figure 2E) and accelerated channel turnover ($t_{1/2} \approx 5.2$ h), ouabain or digoxin failed to further increase the mutant turnover as compared with that of the wild type ($t_{1/2} \approx 3.9$ h; Figure 2F). Collectively these results suggest that the SF mutations can partially rescue the low $[K^+]_{cyt}$ -induced SF collapse and global destabilization of hERG.

Conformational stabilization of the mature hERG potassium channel by cytosolic K⁺

To directly evaluate whether K⁺ can influence the conformational stability of hERG, we examined channel protease susceptibility as a function of [K⁺]. We isolated microsomes containing hERG by differential centrifugation from HeLa cells, yielding predominantly

inside-out PM and right-side-out ER and endocytic vesicles (unpublished data). Because the isolation was performed in nominally K⁺-free sucrose medium, the luminal or extracellular compartment of PM vesicles was assumed to be K⁺-free.

The protease susceptibility of the mature hERG was determined by increasing chymotrypsin or trypsin concentrations in the presence of 75 mM KCl (high K⁺) or N-methyl-D-glucamine (NMDG)-Cl with quantitative immunoblotting. To clamp the microsome's lumen at the extravesicular [K⁺], we performed the protease digestion in the presence of a K⁺-ionophore (valinomycin) and protonophore (carbonyl cyanide *m*-chlorophenylhydrazone [CCCP]). The protease susceptibility was estimated by the protease concentration that was required for 50% elimination of the mature hERG (EC_{50}). At high [K⁺] the trypsin and chymotrypsin resistance of the complex-glycosylated hERG was increased by ~30- and ~3-fold, respectively, relative to that observed in NMDG-Cl medium (Figure 3, A and B). Several additional observations support the notion that K⁺ binding to the mature hERG accounts for the channel conformational stabilization. 1) Nonspecific effects of ion substitution were ruled out by maintaining the osmolality and ionic strength in the low- and high-K⁺ buffers. 2) Similar differences were observed qualitatively with both chymotrypsin and trypsin digestion, ruling out the possibility that the exposure of a single cleavage site accounts for the distinct protease resistance in the presence of K⁺ (Figure 3, A and B). The limited cleavage specificity of chymotrypsin relative to trypsin probably explains the attenuated difference in the observed EC_{50} values for chymotrypsin in low and high K⁺. 3) The SF mutations (F627Y and S641A) enhanced the channel protease resistance to K⁺ depletion (Figure 3C). 4) Other cations known to interact with the hERG selectivity filter (Rb⁺, Cs⁺, and Ba²⁺; Krishnan et al., 2005) rendered protease resistance to the complex-glycosylated hERG (Figure 3E). In contrast, Na⁺ ions, which are unable to bind the SF, failed to stabilize hERG.

The following observation suggests that not only the extravesicular, but also the luminal [K⁺] contributes to the channel stabilization. Maintaining low [K⁺] in the luminal (equivalent to the extracellular) compartment by omitting valinomycin and CCCP during proteolysis reduced the EC_{50} of the mature hERG from ~50 to 7 µg/ml in high-potassium medium (Figure 3, B and D). Further reduction of EC_{50} to 1 µg/ml was observed when the digestion was performed in the NMDG-Cl medium, regardless of the presence of ionophores (Figure 3, B and D). These observations provide direct evidence that both [K⁺]_{cy} and [K⁺]_{ex} can modulate mature hERG conformational stability.

Accelerated internalization, lysosomal targeting, and impaired recycling contribute to glycoside-induced hERG removal from the PM

The PM density of hERG is modulated by the kinetics of internalization, recycling, and lysosomal degradation. We assessed the effect of glycosides on each of these vesicular trafficking steps. Ouabain or digoxin treatment (300 nM for 1.5 h) accelerated hERG internalization by greater than twofold in HeLa and H9C2; cells, as determined by anti-HA Ab uptake assay (Figure 4A). Cardiac glycosides decreased the channel recycling efficiency from early endosomes back to the PM by ~40% (Figure 4B). Recycling of internalized anti-HA-hERG complex was measured with ELISA after blocking the residual cell-surface anti-HA Ab with monovalent Fab secondary Ab as described in Materials and Methods.

Quantitative immunocolocalization showed that endocytosed anti-HA Ab-labeled hERG colocalized with dextran-labeled lysosomes in ouabain-treated cells after 4-h chase (Figure 4C; Manders'

coefficient 56 ± 0.05 vs. control 29 ± 0.04%, $n = 25$). Similarly, hERG colocalized with lysosomes and was largely excluded from early endosomes in ouabain-treated H9C2; cardiac myocytes stained with Lamp1 and EEA1 Abs, respectively (unpublished data and Supplemental Figure 1D). Dissipating the endolysosomal pH gradient with NH₄Cl and baflomycin A1 (Baf) or inhibition of cathepsins with leupeptin and pepstatin partially prevented ouabain-induced hERG degradation (Figure 4D). These observations suggest that lysosomal proteolysis is responsible, at least in part, for rapid degradation of complex-glycosylated hERG upon exposure to glycosides.

To confirm that the destabilized channel is preferentially targeted to lysosomes, we determined the endolysosomal transfer kinetics of internalized hERG. PM-resident hERG channels were labeled with anti-HA Ab and the pH-sensitive, fluorescein isothiocyanate (FITC)-conjugated secondary Fab fragment on ice. After synchronized internalization at 37°C, the pH of hERG-containing vesicles (pH_v) was determined by single-cell fluorescence ratiometric image analysis (FRIA) as a function of chase at 37°C (1–4 h; Barriere et al., 2011). In untreated cells, hERG was largely confined to early endocytic compartments, displaying a mean pH_v of 6.6–6.8 after a 2.5-h chase (Figure 4, E and F), consistent with the immunocolocalization results. Ouabain or digoxin, however, redistributed the channels into more acidic compartments, as indicated by the reduced mean pH_v to 6–6.1 and 5.3–5.1 after a 1.5- and 4-h chase, respectively (Figure 4, E and F). The endolysosomal trafficking of hERG was similarly altered by glycosides in H9C2; cardiac myocytes (Figure 4F, right). H9C2; cells had a slightly lower pH_v of 6.1 in recycling endosomes, as determined by FITC-transferrin and FRIA (Supplemental Figure S1F). Jointly these results show that the combination of accelerated internalization and lysosomal delivery, as well as impeded recycling, is responsible for the glycoside-induced down-regulation of the PM hERG.

Mutations associated with inherited LQT2 destabilize hERG at the plasma membrane

Having established the possible role of the peripheral QC in glycoside-induced hERG PM down-regulation from the PM, we asked whether a similar mechanism might contribute to the loss-of-expression phenotype of G601S and F805C hERG mutants identified in inherited LQT2 syndrome (Furutani et al., 1999; Delisle et al., 2003). Under steady-state conditions, these mutants are preferentially retained at the ER in HeLa and H9C2; cells. Modest expression of complex-glycosylated and PM G601S hERG was detectable by immunoblotting and ELISA, respectively at 37°C (Figure 5, A and B). The mutant PM density was increased by twofold to threefold at reduced temperature (26°C for 48 h) in both HeLa and H9C2; cells (Figure 5, A and B).

The temperature-rescued (r) G601S and F805C channels were functional, as determined by whole-cell patch-clamp electrophysiology (Supplemental Figure S2, A and B). On returning to physiological temperatures (37°C), the rG601S and rF805C hERG were rapidly removed from the PM, as monitored by cell surface ELISA (Figure 5C) and immunofluorescence (Supplemental Figure S2C) in HeLa cells. These results were replicated in a HL-1 mouse cardiac myocyte transient expression system (Supplemental Figure S2E). Both mutations impaired hERG endocytic recycling (Figure 5D). The internalized mutants had profoundly accelerated lysosomal transfer kinetics as compared with their wild-type (wt) counterpart. This was shown by immunostaining (Supplemental Figure S2F) and FRIA in H9C2; and HL-1 cardiac myocytes (Figure 5, E–G), as well as in HeLa cells (Supplemental Figure S3, A–D).

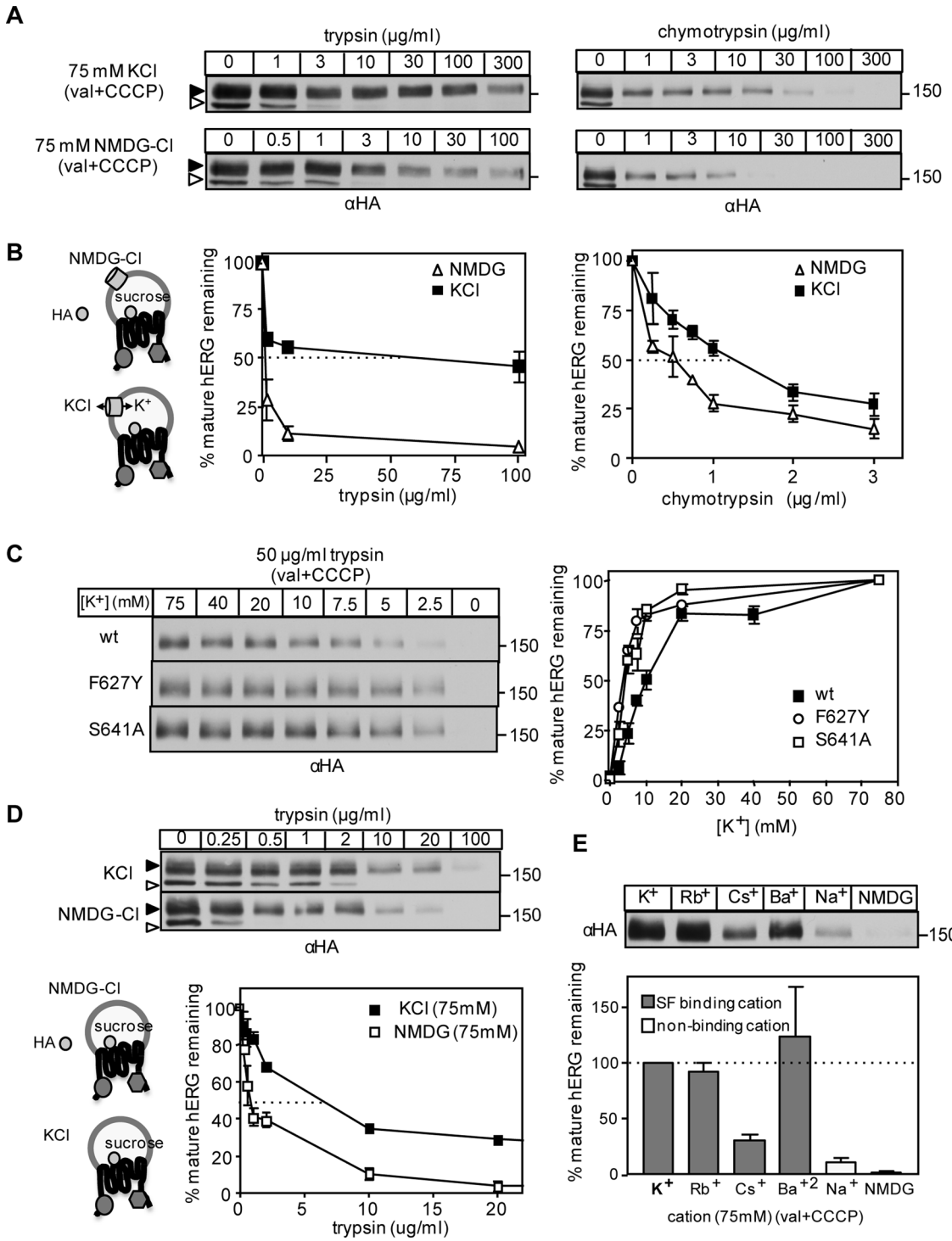


FIGURE 3: Potassium depletion increases hERG protease susceptibility. (A) hERG conformational stability probed with limited proteolysis in concert with immunoblotting using isolated microsomes from HeLa cells. Microsomes were incubated with increasing concentration of chymotrypsin (top) or trypsin (bottom) for 10 min at 35°C in either 75 mM KCl- or 75 mM NMDG-Cl-based medium. Solid arrow, complex glycosylated mature hERG (155 kDa); empty arrow, core-glycosylated hERG. Use of 10 µM valinomycin (val) and 10 µM CCCP facilitated equilibration of luminal [K⁺] with that of the medium (see insert in B). The HA-epitope tag is extracellular and located luminally in microsomes.

(B) Quantitative densitometry of the remaining complex-glycosylated hERG as a function of protease concentration on A. (C) Protease resistance of wt and mutant hERG as a function of [K⁺]. Limited proteolysis in medium with the indicated K⁺ concentration (balance to 300 mOsm with NMDG) and 50 µg/ml trypsin performed as in A. Densitometric analysis of the mature hERG protease resistance was determined on immunoblots (right). (D) Protease susceptibility of hERG at low luminal [K⁺]. Limited proteolysis was performed as in A but in the absence of ionophores to preserve the low intraluminal [K⁺]. Quantification of the mature hERG remaining (bottom). (E) Trypsin (50 µg/ml) digestion was done as in A using either K⁺ or other cations that bind to the selectivity filter (SF). Na⁺ served as a negative control. val, valinomycin.

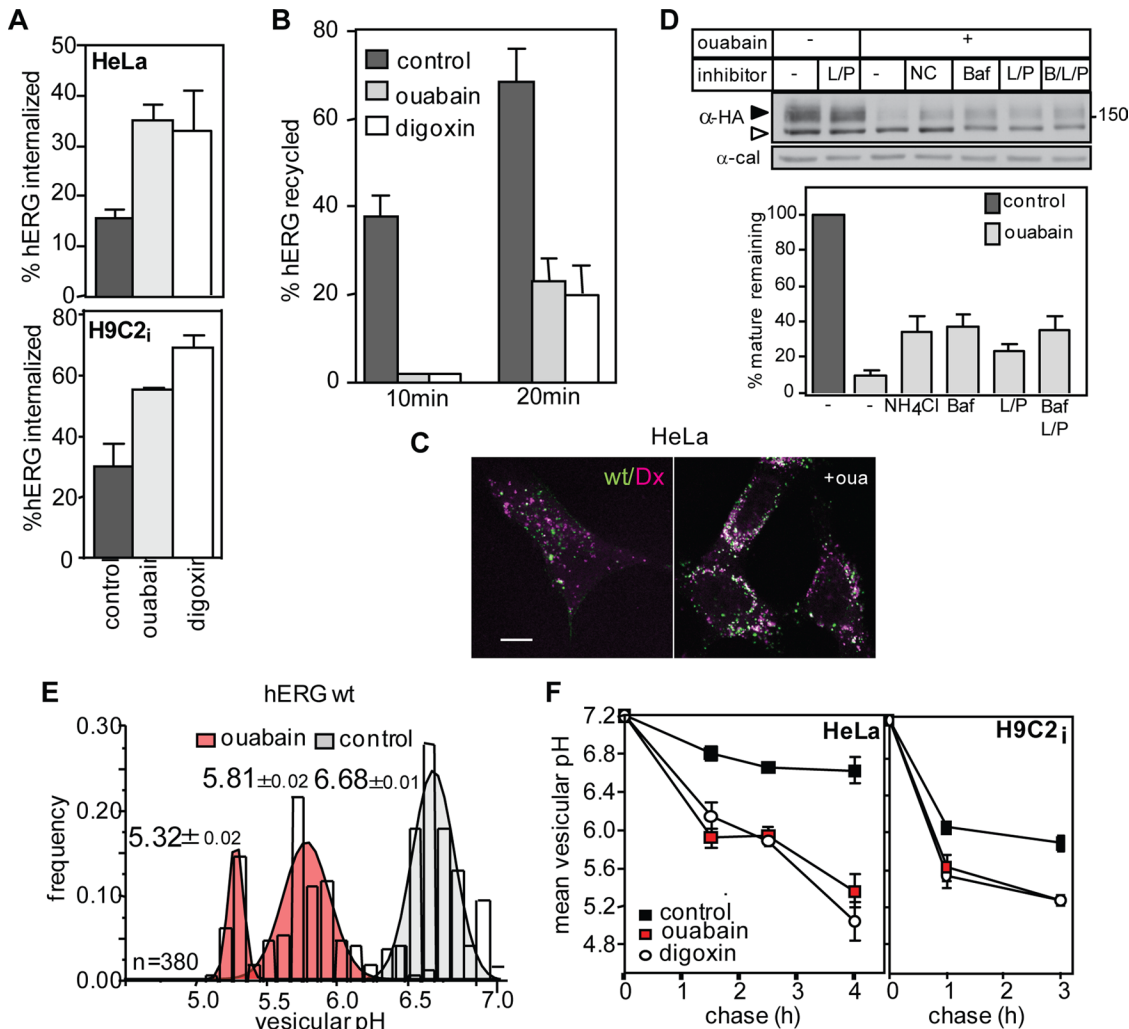


FIGURE 4: Glycosides-induced lysosomal targeting of hERG from the cell surface. (A) Internalization of hERG in HeLa (top) and H9C2_i (bottom) cells was monitored by the Ab uptake assay at 37°C after 1.5-h ouabain or digoxin treatment and measured by cs-ELISA as described in *Materials and Methods*. (B) The recycling efficiency of internalized and anti-HA-labeled hERG was determined by a cs-ELISA as described in *Materials and Methods* and expressed as percentage of endocytosed hERG. (C) hERG is targeted to lysosomes and colocalizes with dextran (Dx) in ouabain-treated cells. Indirect immunostaining of internalized hERG by laser confocal microscopy was visualized in HeLa cells (bar, 10 μ m). Cell-surface hERG was labeled with anti-HA Ab on ice and chased at 37°C in the presence or absence of 300 nM ouabain in Ab-free medium. Texas red-conjugated dextran (50 μ g/ml) was loaded overnight and chased for 4 h. Manders' coefficient for hERG colocalization with dextran was 0.56 \pm 0.08 in ouabain and 0.29 \pm 0.04 in untreated cells ($n = 25$). (D) Immunoblot analysis of hERG degradation after treatment with cycloheximide and 300 nM ouabain in the absence or presence of lysosomal inhibitors baflomycin A1 (Baf), NH₄Cl (NH), and/or leupeptin pepstatin (L/P) for 3 h. Calnexin (cal) served as a loading control, and quantification of mature hERG (solid arrow) is shown in bar graph. (E, F) Histogram (E) and mean pH_v of internalized hERG-containing endocytic vesicles, determined by FRIA in HeLa cells. Anti-HA Ab and FITC-Fab were bound on ice, and FRIA was performed after 1- to 4-h chase in the presence or absence of ouabain or digoxin at 37°C. pH are means \pm SEM. The graph shows the vesicular pH at each chase point (F).

The temperature-rescued, complex-glycosylated G601S channels were more than fivefold more susceptible to trypsinolysis than their wt counterpart (Figure 5H), supporting the notion that conformational destabilization likely contributes to accelerated PM turnover, lysosomal degradation, and loss-of-function phenotype of a subset of LQT2 mutations.

Conformational destabilization provokes hERG polyubiquitination at the PM

We next examined the involvement of ubiquitin (Ub) conjugation in the clearance of conformationally destabilized PM hERG. Postendo-

cytic targeting of rG601S and rF805C hERG was determined after thermal inactivation of the temperature-sensitive E1 Ub-activating enzyme in ts20 cells (Ciechanover *et al.*, 1991; Glzman *et al.*, 2009; Apaja *et al.*, 2010). Exposing ts20, but not E36 cells harboring the wt E1, to nonpermissive temperature rerouted the mutants to early endosomes and impeded lysosomal delivery as determined by FRIA (Supplemental Figure S4, A and B). E1 enzyme inactivation and lysosomal delivery of nonubiquitinated cargoes at nonpermissive temperature have been documented (Apaja *et al.*, 2010), implying that the activity of the ubiquitination machinery is indispensable for lysosomal targeting of PM mutant hERG channels.

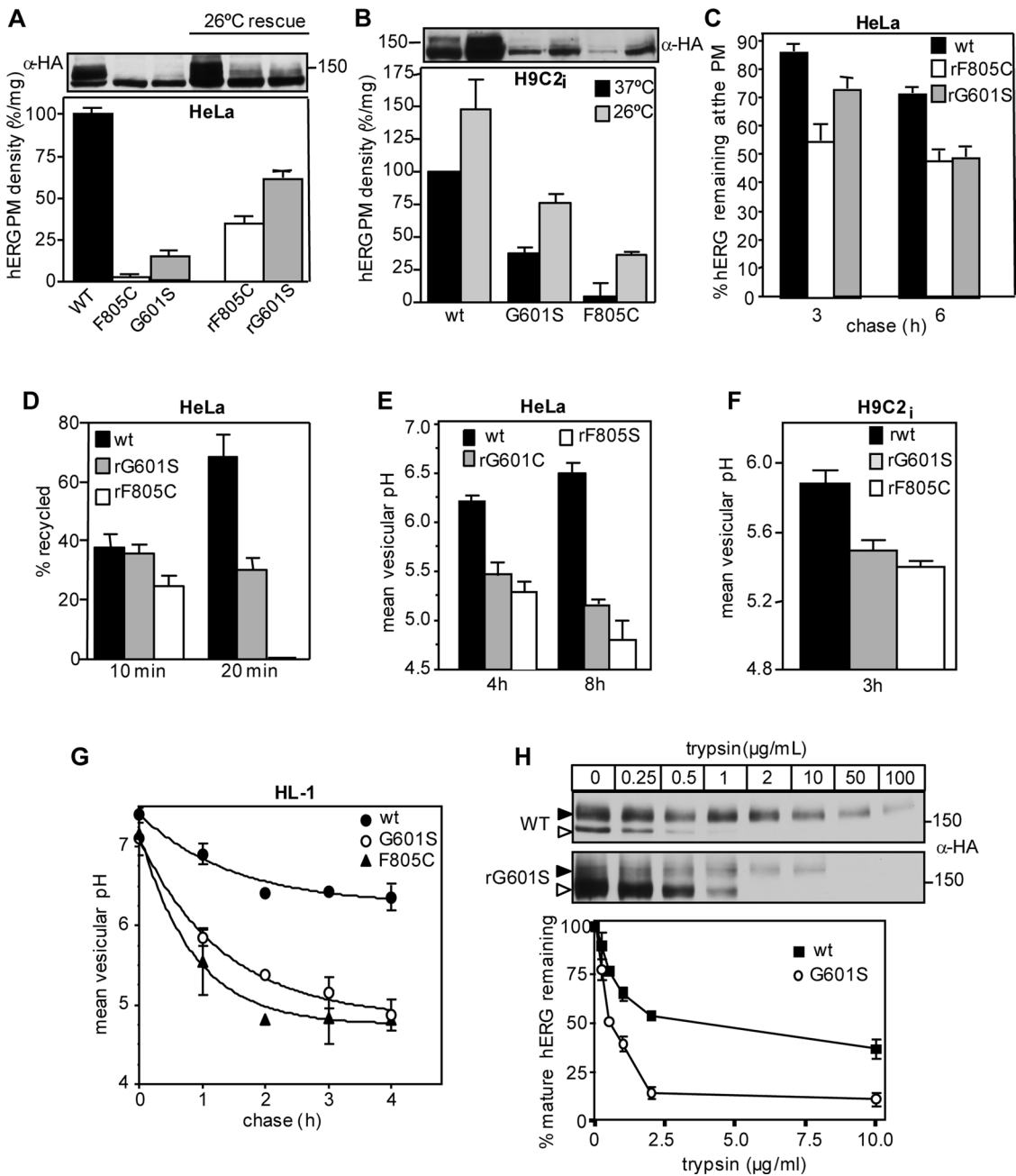


FIGURE 5: LQT2 mutations of hERG are unstable at the PM. (A) Immunoblot analysis of wt, F805C, and G601S hERG expression at 37°C and after 26°C rescue for 48 h (top). PM density of hERG was determined by cs-ELISA as described in Materials and Methods (bottom). (B) Same as in A, but in H9C2_i cells. (C) Stability of rescued (r) hERG was determined at 37°C by cs-ELISA. Rescued channels were unfolded (37°C, 2 h) before cell-surface stability measurements. (D) Recycling efficiency was determined as described in Materials and Methods and expressed as percentage of internalized hERG. The mutants were temperature rescued (r) and unfolded before recycling measurement as in C. (E–G) The luminal pH of vesicles containing rescued and internalized hERG after unfolding (37°C, 2 h) determined in HeLa (E), H9C2_i (F), and HL-1 cardiac myocytes (G) by FRIA as described in Materials and Methods. Anti-HA Ab and FITC-Fab were internalized for 1 h at 37°C, and FRIA was performed after chase at 37°C. (H) Limited trypsinolysis of wt and G601S hERG analyzed by immunoblotting. G601S hERG was rescued at 26°C and then unfolded (37°C, 2 h) before microsome isolation. Densitometric quantification represents three independent experiments (bottom).

To determine the extent of ubiquitination and Ub-chain configuration, we isolated G601S hERG by denaturing immunoprecipitation. On the basis of the partially preserved biosynthetic processing and peripheral instability of the mature G601S in HeLa and H9C2_i cells, we suppressed lysosomal targeting and proteolysis of the endocytosed mutant with Baf. Baf considerably enhanced G601S

ubiquitination, as well as K48- and K63-linked Ub-chain conjugation, detected by Abs recognizing mono- and poly-Ub (P4D1) or the K48- and K63-linked Ub chains, respectively (Figure 6A). The marginal steady-state ubiquitination at 37°C suggests that Ub adducts of neither the immature nor the mature G601S hERG accumulate at detectable levels in the absence of Baf (Figure 6A). Baf inhibition of

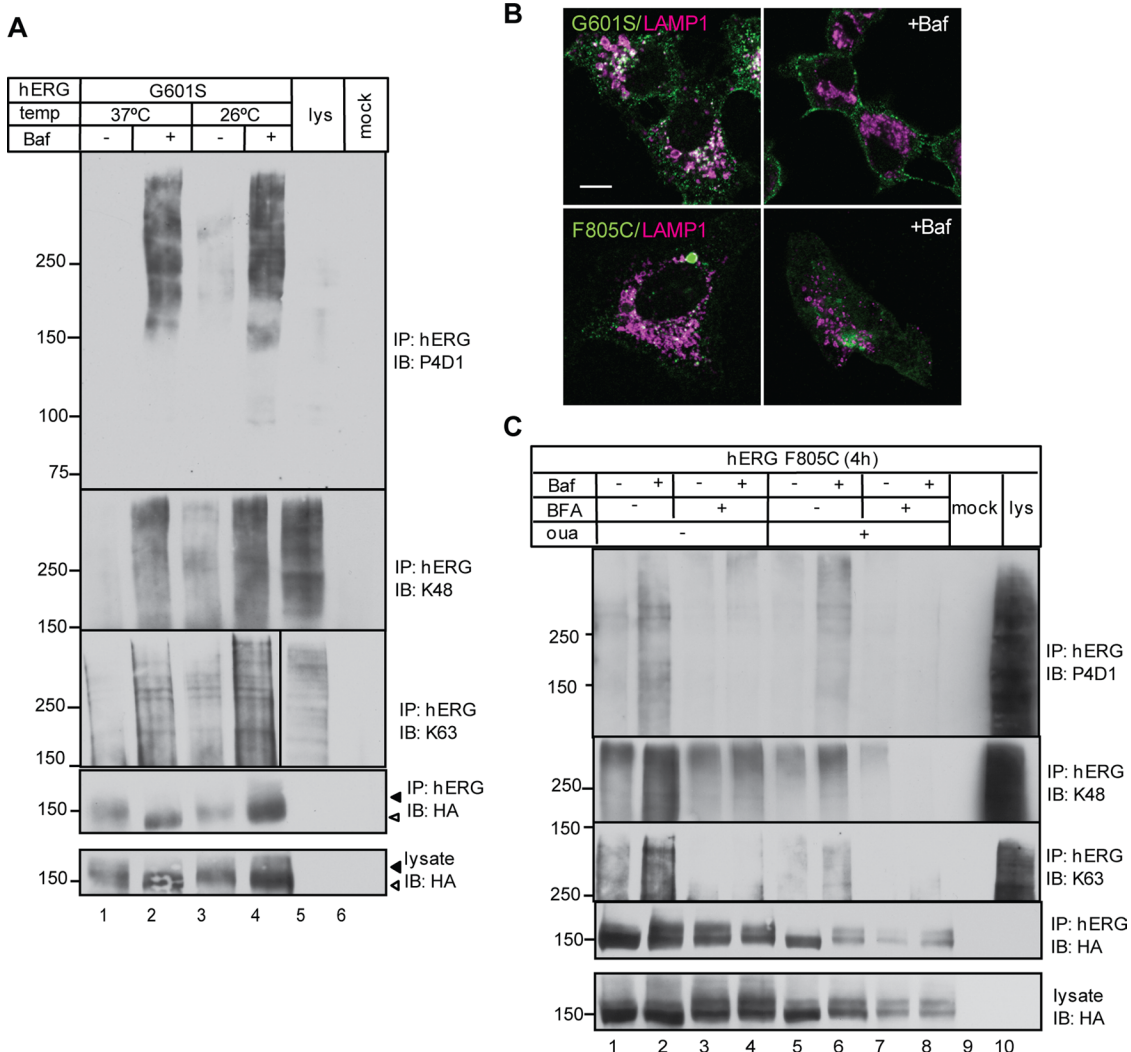


FIGURE 6: Mutant hERGs are ubiquitinated at the PM and post-Golgi compartments. (A) Ubiquitination of G601S hERG was measured by denaturing immunoprecipitation and immunoblotting (IB) using the P4D1 or K63- or K48-linked chain-specific anti-Ub Abs. Cells were treated with Baf and cycloheximide for 3 h at the indicated temperature. (B) Indirect immunostaining and laser confocal microscopy shows PM accumulation of mutant hERG upon lysosomal inhibition. The PM hERG was labeled on ice with anti-HA Ab and chased for 3 h in the presence or absence of Baf. Cells were then fixed and permeabilized, and lysosomes were counterstained for Lamp1. Bar, 10 μ m. (C) Ubiquitination of F805C hERG monitored as in A. ER-to-Golgi transport was inhibited with brefeldin A (4 h).

G601S hERG lysosomal targeting from the PM was confirmed by anti-HA Ab capture in live HeLa cells for 3 h, followed by indirect immunofluorescence (Figure 6B). Baf prevented G601S colocalization with Lamp1 and promoted channel accumulation at the PM (Figure 6B).

For comparison, we also determined the ubiquitination of the F805C hERG, which exhibits more severe ER retention and diminished PM expression than G601S hERG. Whereas Baf promoted F805C hERG ubiquitination (Figure 6C and Supplemental Figure S4C, lanes 1 and 2), this was blunted by inhibiting ER-to-Golgi vesicular transport with brefeldin A (Figure 6C, lanes 3 and 4). Owing to limited ER processing, the subcellular redistribution of F805C hERG from lysosomes to the PM was modest but detectable (Figure 6B). These observations, with the lack of mutant accumulation at the ER upon Baf exposure (Supplemental Figure S4D), imply that Baf primarily interferes with lysosomal proteolysis of the rapidly turning over complex-glycosylated channels that

escaped the ER QC. Jointly these results are consistent with the inference that mutant hERG channels preferentially undergo K63- and K48-linked polyubiquitination in post-Golgi compartments, although multiple monoubiquitination cannot be ruled out.

Next we assessed the ubiquitination of hERG upon ouabain-induced conformational destabilization. hERG ubiquitination was normalized for the amount of immunoprecipitated complex-glycosylated channel, measured by anti-HA immunoblotting. The modest ubiquitination of wt hERG was increased in the presence of Baf or ouabain by 5- and 15-fold, respectively (Figure 7A, lanes 1–3). Baf further augmented the ouabain-induced ubiquitination by twofold, consistent with the notion that ouabain-induced conformational destabilization also provokes mature hERG ubiquitination in post-ER compartments (Figure 7A, lane 4). Baf also enhanced the accumulation of poly-Ub adducts of F805C hERG in ouabain-treated cells, a phenomenon that was suppressed by brefeldin A (Figure 6C, lanes 5–8), in accord with the post-ER origin of ubiquitination.

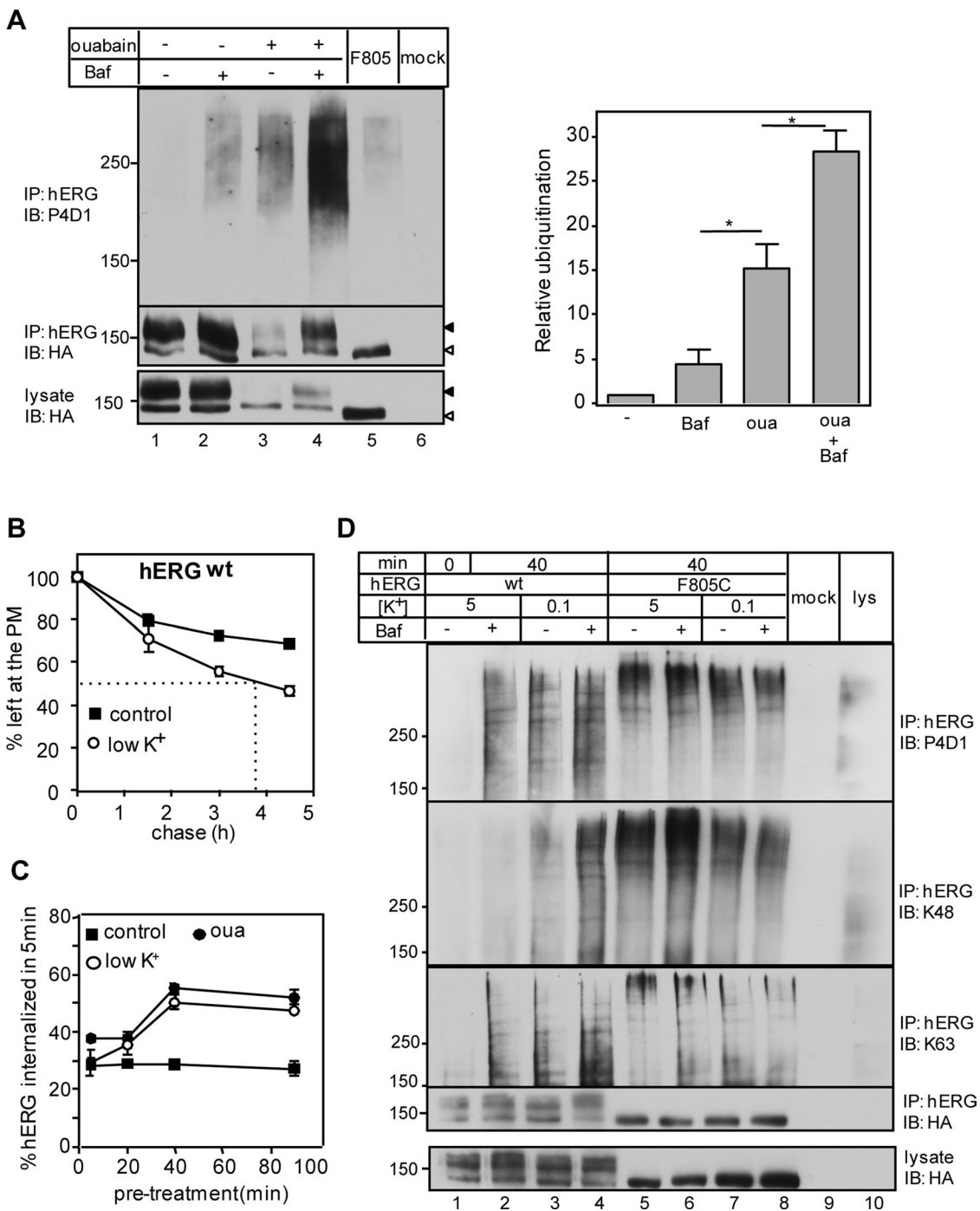


FIGURE 7: Intracellular and extracellular potassium depletion provokes polyubiquitination of mature hERG.
(A) Ubiquitination of wt and F805C hERG in ouabain-treated cells measured as in Figure 6A. Cells were incubated with 300 nM ouabain and 200 nM Baf for 4.5 h. The densitometric ubiquitin signal was normalized to the hERG in the precipitates as detected by anti-HA immunoblotting (right). Data are means \pm SEM, $n = 3$, * $p < 0.05$. **(B)** The PM stability of wt hERG in full medium (5 mM [K⁺]_{ex}) or 0.1 mM [K⁺]_{ex} as determined by cs-ELISA. **(C)** Internalization rate of wt hERG in HeLa cells incubated in 300 nM ouabain, 0.1 mM [K⁺]_{ex}, or complete medium for the indicated time determined using cs-ELISA. **(D)** Effect on 0.1 mM and 5 mM [K⁺]_{ex} in the absence or presence of Baf on wt and F805C ubiquitination determined after 40-min incubation, as in A.

Extracellular hypokalemia elicits hERG polyubiquitination

Extracellular hypokalemia acutely inactivates hERG, followed by the channel monoubiquitination-dependent removal from the PM, which is completed in 6 h (Guo et al., 2009). Because long-term extracellular hypokalemia may lead to intracellular K⁺ depletion

(Figure 1E), we limited [K⁺]_{cyt} depletion by applying extracellular hypokalemia (0.1 mM) for 40 min before measuring ubiquitination. This approach elicited only 25 and 20% reductions in the cellular K⁺ content and hERG PM density, respectively (Figures 1E and 7B) while increasing the internalization rate by twofold (Figure 7C). Low

$[K^+]_{\text{ex}}$ induced hERG polyubiquitination, as indicated by immunoblotting with the K48- or K63-linked Ub-chain-specific and P4D1 Abs (Figure 7D, lanes 1 and 3). Ubiquitination of hERG under low $[K^+]_{\text{ex}}$ is augmented in the presence of Baf, supporting the observation that extracellular hypokalemia downregulates hERG via lysosomal proteolysis (Guo et al., 2009; Massaeli et al., 2010a; Sun et al., 2011). No major effect was observed on F805C under the same conditions (Figure 7D, lanes 5–8). These observations, together with the enhanced protease susceptibility of hERG upon luminal K^+ depletion (Figure 3D), suggest that K^+ contributes to the channel structural stabilization both at the extracellular and cytosolic sites.

CHIP- and ESCRT-dependent disposal of nonnative hERG from cell surface

CHIP is a chaperone-dependent quality control E3 Ub ligase that has been implicated in the ubiquitination of nonnative membrane proteins at both the ER and the PM (Meacham et al., 2001; Apaja et al., 2010; Okiyone et al., 2010; Walker et al., 2010). The involvement of CHIP in hERG quality control was assessed using lentiviral short hairpin RNA (shRNA)-mediated knockdown in HeLa cells, which was verified by immunoblotting (Supplemental Figure S5A). CHIP ablation increased the abundance of mature G601S and F805C hERG in post-ER and PM compartments (Figure 8A and Supplemental Figure S5B). This was at least partly due to decreased internalization (Figure 8, B and C) and rerouting of mutants from lysosomes to early endosomes and multivesicular bodies (MVBs) during a 4-h chase (Figure 8, D and E). Thus both impeded internalization and delayed lysosomal degradation account for the mutant stabilization in shCHIP-treated cells.

CHIP ablation partially suppressed ouabain- or digoxin-induced hERG disposal from the PM (Figure 8F). Of importance, neither the K30A CHIP mutant, which is unable to bind Hsc70/Hsp90, nor catalytically inactive H260Q CHIP overexpression could restore rapid internalization and PM turnover of the ouabain-treated hERG in HeLa cells depleted of endogenous CHIP by shCHIP (Figure 8, G–I). This result supports the notion that chaperones are required for CHIP-mediated down-regulation of hERG upon glycoside-induced misfolding at the PM, a substrate recognition mechanism demonstrated for multiple QC substrates of CHIP (Connell et al., 2001; Meacham et al., 2001). The CHIP ablation effect could be attributed to CHIP-dependent ubiquitination of hERG, since siCHIP reduced ouabain-induced polyubiquitination of wt-hERG (Figure 9A, lanes 3 and 6, and Supplemental Figure S5D). A similar effect was observed on K48- and K63-linked Ub-chain conjugation to G601S hERG (Figure 9B, lanes 1, 2, 5, and 6, and Supplemental Figure S5E), suggesting that CHIP is partly responsible for hERG down-regulation in the presence of mutations or cardiac glycosides. Ablation of the neural precursor cell-expressed developmentally down-regulated protein 4 long isoform (Nedd4-2) E3 ligase, which associates with the C-terminal PY motif of hERG (Albesa et al., 2011), failed to counteract the metabolic instability in the presence of glycosides or hERG mutations (Supplemental Figure S5, C and F, and unpublished data). Furthermore, broad-specificity inhibitors of protein kinase A (PKA) or protein kinase C (PKC) failed to stimulate hERG down-regulation in the presence or absence of ouabain (unpublished data), suggesting that glycoside-induced down-regulation of hERG is independent of PKA- and PKC-dependent phosphorylation.

If ubiquitination serves as a sorting signal for nonnative hERG disposal from the PM via lysosomal proteolysis, it is reasonable to assume that Ub-binding constituents of the ESCRT machinery are critical in targeting the channel into MVB/lysosomes (Apaja et al., 2010; Henne et al., 2011). This possibility was tested by measuring

the lysosomal transport kinetics of conformationally destabilized hERG in cells with ablated ESCRT0 (Hrs and Stam) or ESCRT1 (Tsg101) components. Both mutant hERGs and the glycoside-treated wt hERG remained associated with early/recycling endosomes, as indicated by their pH_v of 6.3–6.4 in ESCRT0 or I-depleted cells (Figure 10, A–C). Hrs, Stam1, or Tsg101 ablation profoundly attenuated the rapid PM removal of wt hERG in ouabain- or digoxin-treated cells (Figure 10D). shRNA treatment, however, had no influence on the lysosomal delivery of FITC-labeled CD63/Lamp2 or dextran (Figure 10B, right). Collectively these results indicate that both intracellular K^+ depletion and LQT2 mutations enhance the ubiquitination of mature hERGs in a CHIP-dependent manner, a prerequisite for nonnative channel ESCRT-dependent lysosomal delivery (Figure 10D).

DISCUSSION

Here we propose that structurally defective hERG represents a newly identified substrate of the peripheral QC machinery, thereby contributing to the hERG loss-of-expression phenotype at the PM and the pathogenesis of a subset of LQT2 syndromes.

Accelerated removal of mutant hERG from the PM contributes to the expression defect in a subset of inherited LQT2 syndrome

More than 60% of ~200 LQT2-associated missense mutations interfere with conformational maturation of hERG channels (Anderson et al., 2006). Depending on the severity of the folding defect and the engagement of multiple ER QC mechanisms (Brodsky and Skach, 2011), newly synthesized membrane proteins can be completely or partially retained at the ER (Haardt et al., 1999; Arvan et al., 2002; Glzman et al., 2009; Apaja et al., 2010). Whereas F805C hERG ER maturation efficiency and PM turnover are compromised (Figure 5), the G601S (Figure 6) and other missense mutations in the PAS domain (e.g., R56Q, C64Y, T65P; Harley et al., 2012; Ke et al., 2013) more efficiently escape from the ER QC and are expressed at the PM. It is plausible that destabilization of the PAS domain renders the PAS mutants conformationally defective and they become susceptible to CHIP-dependent ubiquitination similar that to G601S and F805C hERG, underlying the significance of the peripheral QC in the pathogenesis of inherited LQT2 syndrome.

Conformational destabilization of hERG by intracellular or extracellular hypokalemia leads to acquired LQT2 phenotype

$[K^+]_{\text{cy}}$ depletion caused by cardiac glycosides was postulated to impair the conformational maturation of newly translated hERG (Wang et al., 2009). Here we extend the paradigm of cardiac glycoside action and show that $[K^+]_{\text{cy}}$ depletion can conformationally and metabolically destabilize mature hERG at the PM and post-Golgi compartments (Figures 2 and 3).

Of note, $[K^+]_{\text{ex}}$ is also required to maintain hERG in a structurally and functionally native state. Extracellular hypokalemia induces loss of channel activity with $t_{1/2} \approx 1$ min from the PM, which is recovered with $t_{1/2} \approx 20$ min at 5 mM $[K^+]_{\text{ex}}$ (Massaeli et al., 2010a). Long-term hypokalemia, however, triggers channel irreversible loss by metabolic down-regulation with $t_{1/2} \approx 3$ h (Sanguinetti et al., 1995; Guo et al., 2009; Massaeli et al., 2010b), a process that is initiated ~40 min after the onset of hypokalemia (Figure 7, B and C). Given the similar metabolic fate, enhanced endocytosis, and ubiquitination of complex-glycosylated hERG upon $[K^+]_{\text{ex}}$ or $[K^+]_{\text{cy}}$ depletion, we propose that both $[K^+]_{\text{cy}}$ and $[K^+]_{\text{ex}}$ play permissive and synergistic roles in structural stabilization of mature hERG at the PM, a conclusion supported by the decreasing protease resistance of

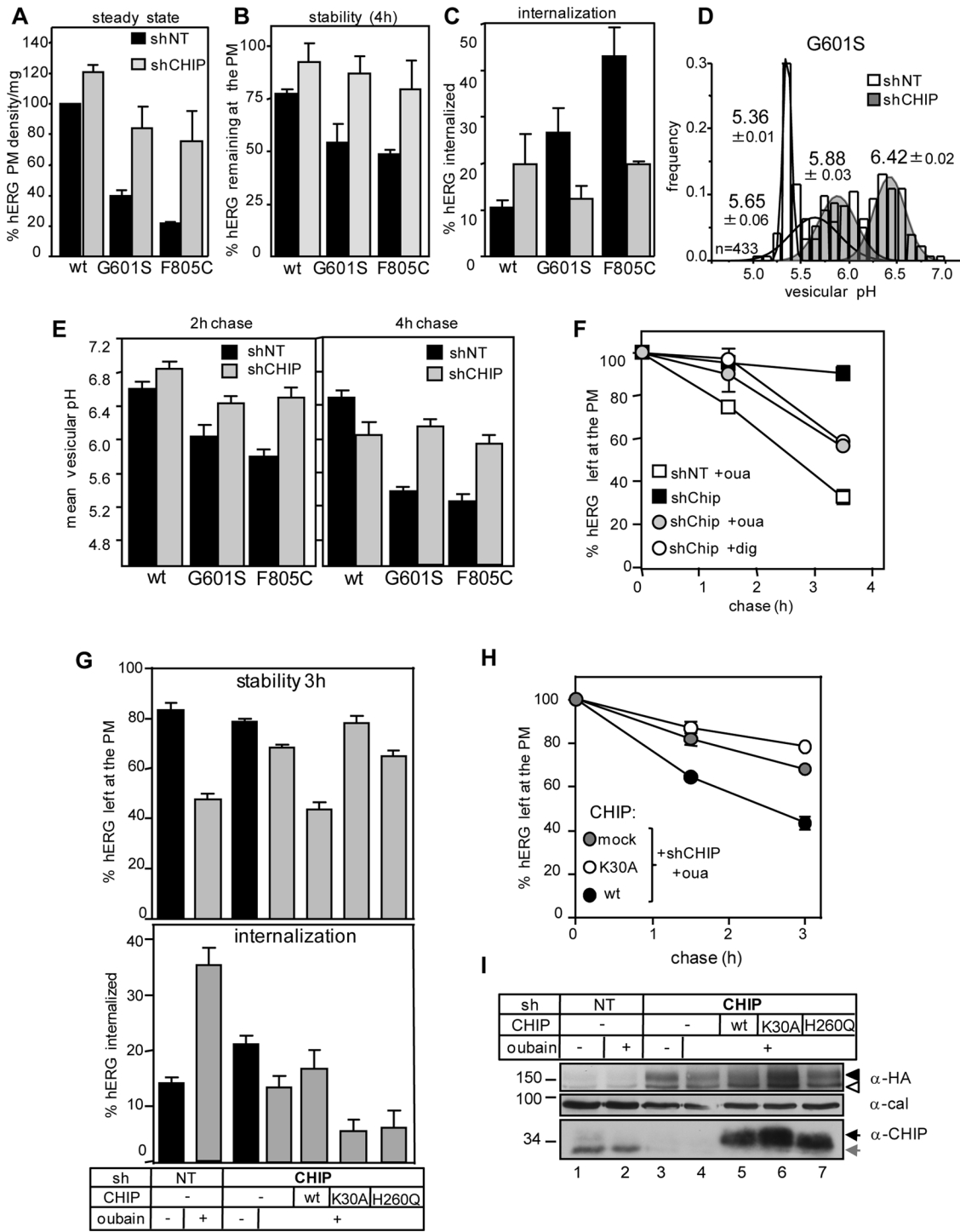


FIGURE 8: Role of CHIP in the ubiquitin-dependent peripheral destabilization of hERG channel. (A, B) The wt, G601S, and F805C hERG PM density (A) and stability (B) determined after 4-h chase in shCHIP cells by cs-ELISA. (C) Internalization rate of hERG was monitored at 37°C. Internalization was determined by Ab uptake in shCHIP cells for 5 min. (D) Representative results of pH_v histogram of G601S hERG-containing vesicles in shCHIP or shNT HeLa cells after 4-h chase. The mean pH_v of the individual components of multiple Gaussian distribution is indicated from a total of 433 vesicles. (E) Mean pH_v of wt, G601S, and F805C hERG in shNT and shCHIP-depleted cells measured after anti-HA Ab and FITC-Fab internalization for 1 h and chased for 2 or 4 h. hERG-expressing cells were rescued at 26°C and then unfolded (37°C, 2 h) before Ab labeling. (F) The wt hERG disappearance kinetics from the PM in shCHIP and shNT HeLa cells treated with ouabain or digoxin. hERG PM density was determined by cs-ELISA. (G, H) PM turnover of hERG was measured as in F, but shCHIP-expressing HeLa cells were overexpressed with wt, K30A (incapable of chaperone binding), or H260Q (catalytically inactive) myc-CHIP variant. (I) Immunoblotting of cells depicted in G and H using anti-HA and anti-CHIP Abs for detecting hERG, endogenous (gray arrow), and myc-CHIP (black arrow), respectively. Calnexin (cal) was used as loading control.

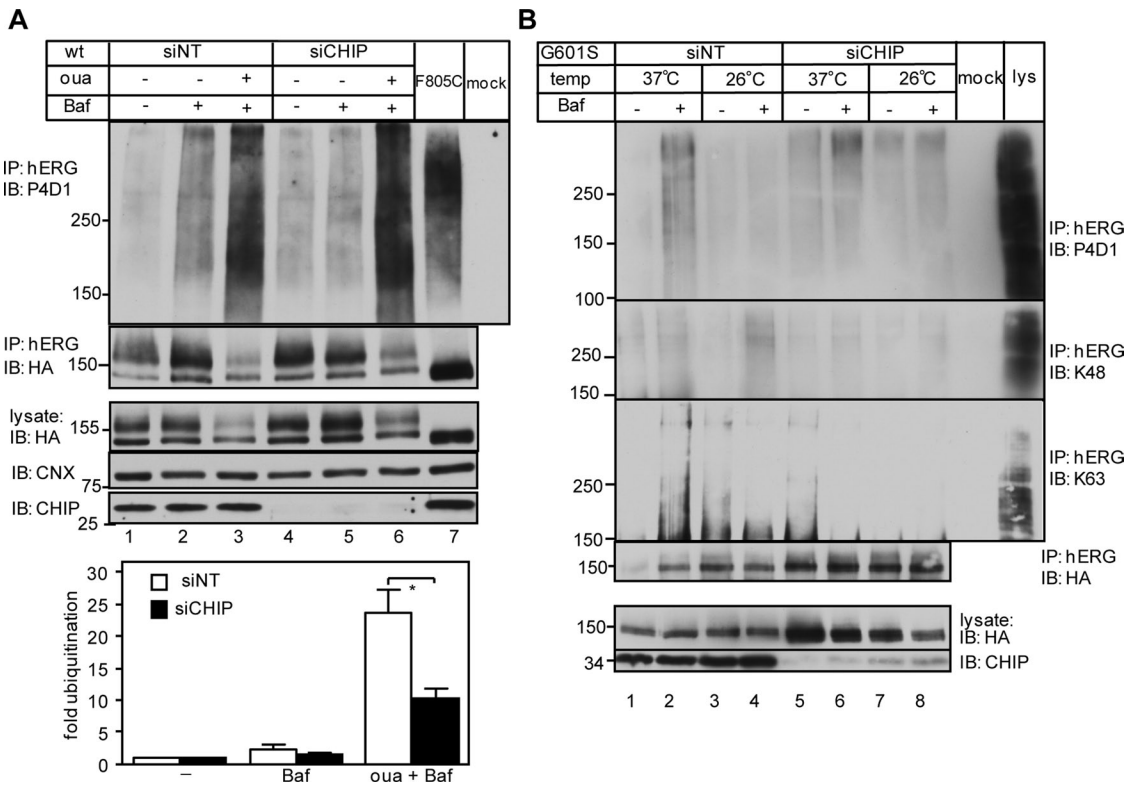


FIGURE 9: Ubiquitin-dependent peripheral removal of hERG channel. (A, B) Effect of siCHIP on ouabain-induced ubiquitination of wt (A) and G601S hERG (B). Denaturing immunoprecipitation and Ub detection were performed as in Figure 6A. In G the densitometric analysis of ubiquitination at molecular weight >150 kDa was normalized to complex-glycosylated hERG. Data are means \pm SEM, $n = 3$, * $p < 0.05$. dig; digoxin; oua; ouabain.

complex-glycosylated hERG in microsomes upon $[K^+]$ depletion of the luminal and the extravesicular compartment (Figure 3). Furthermore, cations that interact specifically with hERG SF, but not Na^+ , prevent K^+ depletion-induced PM down-regulation (Massaeli et al., 2010a) and conformation destabilization (Figure 3).

Previous work showed that the SF of KcsA, a prototypical K^+ channel, adopts a collapsed conformation upon loss of K^+ binding, probably due to enthalpic destabilization of the SF (Lockless et al., 2007). A similar mechanism may prevail for the hERG SF, with significant sequence homology to that of the KcsA (Zhou and MacKinnon, 2003). In support of this conjecture, mutations (e.g., F627Y) within or in the vicinity of the SF desensitize hERG PM metabolic and structural destabilization in response to either intracellular or extracellular K^+ depletion (Figures 2 and 3; Wang et al., 2009; Massaeli et al., 2010a).

How the K^+ -depleted SF conformation differs from the C-type inactivated state (which is believed to involve SF closure) remains to be established. hERG inactivation involves multiple transmembrane and cytosolic domains, suggesting that the SF is conformationally coupled to the rest of the channel (Wang et al., 2011; Gustina and Trudeau, 2013). One possible scenario is that, at reduced $[K^+]$, extended residence in the inactivated state allows allosteric unfolding of multiple hERG domains (Figure 10E).

Several drugs have been identified to cause LQT2 syndrome by disrupting hERG biosynthetic trafficking rather than blocking channel conductance, presumably by imposing either a thermodynamic or a kinetic defect in the folding pathway (Dennis et al., 2007, 2011, 2012). A more complex mechanism of action was identified for the antidepressant desipramine, causing both ER retention and

polyubiquitination-dependent rapid lysosomal degradation of the channel from the PM (Dennis et al., 2011). Thus desipramine, similar to a variety of other drugs, may introduce a conformational defect in hERG that is recognized by the peripheral QC machinery.

The role of CHIP in misfolded hERG ubiquitination at the PM

Here we identified CHIP as an E3 ubiquitin ligase involved in the regulation of nonnative hERG at the PM. CHIP recruitment to non-native hERG is probably mediated via Hsc/Hsp70/Hsp90 binding to exposed hydrophobic residues that are otherwise buried in the native channel, similar to that described for other misfolded ER, cytosolic, and PM polypeptides (Cyr et al., 2002; Apaja et al., 2010; Okiyone et al., 2010). This conclusion is supported by the observation that disruption of Hsp70/Hsp90 binding to CHIP prevented CHIP-mediated down-regulation of hERG from the PM. Although the Nedd4-2 E3 ligase had no discernible role in hERG QC at the PM (Supplemental Figure S5 and unpublished data), Nedd4-2 appears to be involved in second-messenger-mediated regulation of hERG PM density by associating with the C-terminal PY motif (Henke et al., 2004; Maier et al., 2006; Boehmer et al., 2008; Lamothe and Zhang, 2013).

It is intriguing that monoubiquitination was implicated in the extracellular hypokalemia-induced down-regulation of PM hERG (Sun et al., 2011). In contrast, we show that hERG becomes susceptible to K48- and K63-linked polyubiquitination, although multiple monoubiquitination and other Ub-chain configurations cannot be ruled out. The documented CHIP-dependent polyubiquitination of hERG, regardless of whether structural destabilization was attained

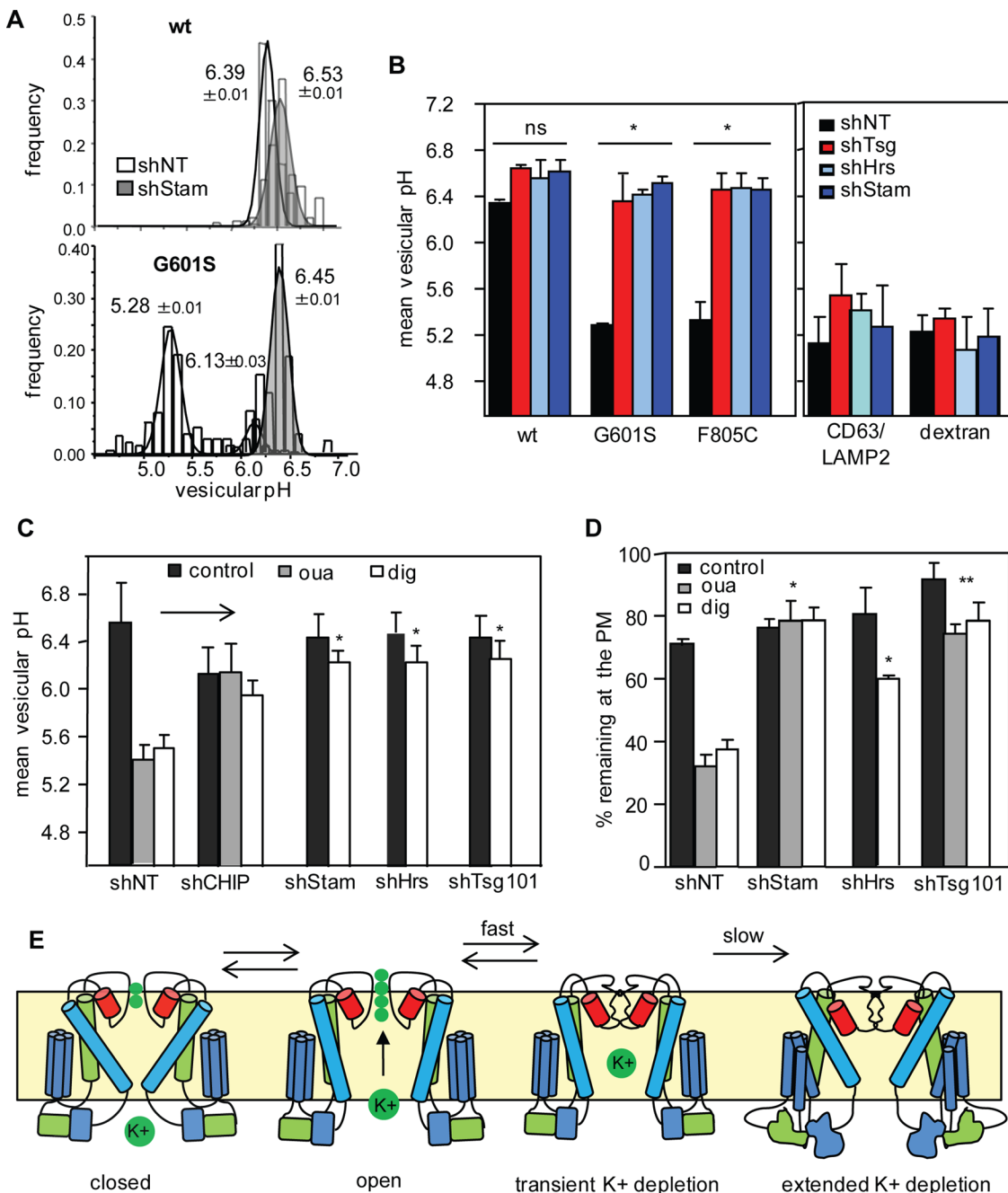


FIGURE 10: ESCRT0-I is required for nonnative hERG degradation from the PM. (A) Representative pH_v histograms of internalized wt and G601S hERG containing vesicles after 4-h chase in shNT and shStam1 cells determined with FRIA. hERG was rescued at 26°C and then unfolded (37°C, 2 h). Anti-HA Ab and FITC-Fab were internalized for 1 h at 37°C before the chase in Ab-free medium. (B) The mean vesicular pH of hERG-containing compartments was determined after 4-h chase in cells depleted for Tsg101, Hrs, and Stam1 (left). The lysosomal targeting of CD63/LAMP2 and dextran was not influenced by shESCRTs (right). (C) The mean pH_v of internalized wt hERG-containing compartment after ouabain or digoxin treatment for 3.5 h in HeLa cells depleted for Tsg101, Hrs, and Stam1. (D) Cell-surface stability of hERG in ouabain- or digoxin-treated shESCRt cells determined with cs-ELISA after 3.5-h chase. (F) Schematic model of hERG gating cycles and the effect of K⁺ depletion on hERG conformation. Significance was calculated against NT or treated shNT. Data are means ± SEM, $n \geq 3$; * $p \leq 0.05$ and ** $p \leq 0.01$.

by missense mutations or extracellular/intracellular K⁺ depletion, suggests that the conformational defect recognized by the QC converges onto to the cytosolic domains.

In light of the different cellular expression systems used, we can only speculate about the underlying cause of the monoubiquitination of hERG upon low [K⁺]_{ex} exposure (Sun et al., 2011). Whereas

we used a direct immunodetection method of hERG ubiquitination with three validated poly-Ub-specific antibodies after denaturing precipitation, the conclusion of Sun et al. (2011) was primarily based on channel turnover measurements in cells overexpressing the Lys-less Ub in order to prevent substrate polyubiquitination. Because even a limited initial incorporation of endogenous Ub would permit

Ub-chain elongation and clearance of hERG, one explanation is that polyubiquitination of hERG was only partially inhibited. This possibility is in line with incomplete suppression of β -cateinin polyubiquitination by Lys-less Ub overexpression, as shown in Figure 2B-c in Sun et al. (2011).

K48- and K63-linked linear and forked polyubiquitination is a hallmark of CHIP activity (Kim et al., 2007) and is in line with the reported polyubiquitination pattern of destabilized hERG upon K^+ depletion (Figure 8) or desipramine treatment (Dennis et al., 2011). Accumulating evidence indicates that efficient endolysosomal sorting of membrane cargoes requires K63-linked polyubiquitination to increase the avidity of endocytic Ub-binding adaptors binding to cargo (Barriere et al., 2006; Hawryluk et al., 2006; Boname et al., 2010; Ren and Hurley, 2010). Partial inhibition of both polyubiquitination and down-regulation of PM hERG by siCHIP may be accounted for by the redundancy of E3 ligases in the PM QC, as observed for multiple cellular QC machineries (Arvan et al., 2002; Brodsky and Skach, 2011; Okiyoneeda et al., 2011), and warrants further investigation to identify possible therapeutic targets in conformational diseases.

MATERIALS AND METHODS

Plasmids and transfection

The wt, G601S, and F805C hERG expression constructs have been described previously (Walker et al., 2007, 2010). The selectivity filter mutations F627Y and S641A were engineered by overlapping PCR and inserted as a *Bst*II-*Sbf*I fragment. All hERG constructs contain an HA tag in the first extracellular loop that does not interfere with processing and function (Akhavan et al., 2003). Myc-CHIP constructs have been described previously (Apaja et al., 2010).

HeLa and HEK cells constitutively expressing hERG variants were generated by lentiviral transduction using the pTZV4-CMV-IRES-puro (Open Biosystems, Pittsburgh, PA) plasmid, and selection was maintained in 1 μ g/ml puromycin. Lentivirus was produced as described previously (Apaja et al., 2010). The parental H9C2 rat cardiac myocyte cell line containing the Tet-On transactivator (H9C2 $_t$) was generated using the Lenti-X Tet-On Advanced Inducible Expression System (Clontech, Carlsbad, CA). Highly inducible clonal cell populations were selected after fluorescence-activated cell sorting of the doxycycline-treated and transiently transfected cells with inducible pcDNA5-GFP. For generating inducible hERG (hERG $_i$), H9C2 $_t$ cells were transduced with the pLVX-Tight-Puro (Clontech) vector encoding the hERG variants, and mixtures of clones were selected in the presence of 1 μ g/ml puromycin and 300 μ g/ml G418. Lentiviruses for encoding the transactivator and hERGs were produced using the Lenti-X HT Packaging System (Clontech) in HEK293T cells according to the manufacturer's instructions. Transgene expression was induced in the presence of doxycycline (0.5 μ g/ml; Sigma-Aldrich, Oakville, Canada) for 48 h at 37°C. Transient transfection of HeLa or H9C2 cells was carried out using Lipofectamine 2000 (Life Technologies, Carlsbad, CA) 48 h before analysis. Cells were cultured in DMEM containing 10% fetal bovine serum and antibiotics to maintain selection pressure.

RNA interference

Doxycycline-inducible (pTRIPZ) lentivirus vectors encoding shRNAmir-adapted shRNA specific for CHIP (V2THS_208833), Stam (V2THS_172428), Hrs (V2THS_36954), and Tsg101 (V3THS_305572) or nontargeted variant (NT; ATCTCGCTGGCGAGAGTAAG) were obtained from Thermo Scientific, Open Biosystems. Lentiviruses were produced and HeLa cells were infected as described Apaja et al. (2010). The knockdown efficiency of target protein was determined by immunoblotting. Small interfering RNA (siRNA)

SMARTpools to human CHIP (NM_005861) and NEDD-4-2 (NEDD4L, NM_015277) and nontarget siRNA (UAGCGACUAAACACAUCAA, D-001210-01) were purchased from Thermo Scientific Dharmaco (Rockford, IL). HeLa cells were transfected with 50 nM siRNA using Oligofectamine (Invitrogen). When indicated, hERG channels were temperature rescued at 26°C for 24 h.

Electrophysiology

The hERG current (I_{hERG}) was recorded with an Axopatch 200B amplifier (Axon Instruments, Sunnyvale, CA) coupled with a CV 203BU headstage in the whole-cell patch clamp mode. To ensure adequate voltage control, a minimum of 80% series resistance compensation was required along with an access resistance <10 M Ω . Command pulses were generated by a Digidata 1440A controlled by pClamp 10.2 software (Axon Instruments). Depolarizing steps (7 s) were imposed from a -80 mV holding potential in increments of 10 mV up +70 mV, followed by a step back to -50 mV (2 s), which provoked the tail currents. Subsequently, the membrane was clamped back to -80 mV holding potential for 1 s before the next depolarizing step. Data were acquired at 20 kHz and was low-pass filtered at 2 kHz. Nonlinear curve fitting was performed using Clampfit 10.2 to determine peak tail current amplitudes. All current values were normalized to cellular capacitance (picofarads).

Borosilicate glass pipettes (Warner Instruments, Hamden, CT) were prepared with a microprocessor-controlled, multistage puller (P97; Sutter Instruments, Novato, CA) to produce tip resistance of 2–4 M Ω when filled with 135 mM KCl, 5 mM ethylene glycol tetra-acetic acid, 1 mM MgCl₂, and 10 mM 4-(2-hydroxyethyl)-1-piperazineethanesulfonic acid (HEPES), pH 7.2 with KOH; 300 mOsm. Cells were plated in the perfusion chamber of an inverted microscope (Zeiss Axiovert S100TV) and perfused using a gravity-based flow system (1–2 ml/min) containing Tyrode's solution (135 mM NaCl, 5 mM KCl, 1 mM CaCl₂, 1 mM MgCl₂, 10 mM HEPES, 10 mM glucose; pH 7.4 with NaOH; 300 mOsm). All experiments were performed at room temperature.

Cell surface density, internalization, and metabolic stability measurements of hERG at the cell surface and endocytic pathway

Cell-surface density, internalization, and stability were monitored by taking advantage of the extracellular HA epitope of hERG, using cell-surface ELISA-based methodologies as described earlier (Apaja et al., 2010). Briefly, the extracellular HA epitope was labeled with mouse monoclonal anti-HA Ab (1:1000 dilution; Covance, Canada) and detected with horseradish peroxidase (HRP)-conjugated secondary Ab (Amersham Biosciences, Canada) in conjunction with Amplex Red fluorogenic substrate (Life Technologies). The fluorescence signal was measured from quadruplicate samples using a POLARstar OPTIMA (BMG Labtech, Germany) or a Tecan Infinite M1000 (Tecan Group, Switzerland) fluorescence plate reader with 544-nm excitation and 590-nm emission. Mock-transfected cells served to determine nonspecific Ab binding. hERG internalization and stability were calculated from the loss of the initially labeled hERG PM pool after a chase period of 5 min to 4 h, respectively, and expressed as percentage of the initial hERG density.

Recycling assay

hERG recycling assay was based on the detection of exocytosis of the internalized Ab-hERG complex. Anti-HA Ab detection was performed as described for the cell-surface density assay. Anti-HA Ab (1:1000, c11; Covance)-hERG complex was internalized for 20 min at 37°C. hERG-Ab complexes remaining at the PM

were blocked with mouse monovalent F(ab')₂ fragments (1:100; Jackson ImmunoResearch Laboratories, West Grove, PA) on ice. Recycling was activated for 10–20 min at 37°C. Exocytosed Ab-hERG complexes were measured by cell-surface ELISA. Non-specific Ab background, as well as the residual signal derived after F(ab')₂ blocking, was taken into account when calculating hERG recycling efficiency, expressed as percentage of the endocytosed pool.

Immunoprecipitation and protein analyses

For immunoblotting, cells expressing hERG were solubilized in Triton X-100 lysis buffer (1% Triton X-100, 25 mM Tris-Cl, 150 mM NaCl, pH 8.0, 10 µM MG132 [Cayman Chemical, Ann Arbor, MI] containing 20 µM PR-619 [Lifesensors, Malvern, PA], 10 µg/ml pepstatin + leupeptin, 1 mM phenylmethylsulfonyl fluoride, and 5 mM N-ethyl-maleimide) on ice. Treatment with cycloheximide (150 µg/ml; Sigma-Aldrich), ouabain, and digoxin (300 nM if not otherwise indicated; Sigma-Aldrich) was carried out in full medium at 37°C. Lysosomal trafficking was inhibited by adding Baf (200 nM; LC Laboratories, Woburn, MA) or 10 mM NH₄Cl for 4 h at 37°C or with 10 µM leupeptin/pepstatin for 16 h at 37°C.

To measure hERG ubiquitination, HeLa cells were lysed, and proteins were denatured with 1% (wt/vol) SDS for 5 min. After 10-fold dilution of the denaturing lysis buffer, hERG was precipitated with polyclonal anti-hERG Ab (1:200, C-terminus epitope; Millipore [Billerica, MA] or Alomone Laboratories [Israel]) on protein G-agarose or Dynabeads (Life Technologies). The precipitates were probed for hERG and ubiquitin using monoclonal anti-HA, P4D1 anti-ubiquitin (Santa Cruz Biotechnology, Dallas, TX), Apu2 (K48 Ub-chain specific), or Apu3 (K63 Ub-chain specific) Abs (Millipore), respectively.

Biotinylation of cell-surface proteins was performed on HeLa cell monolayer by incubating with 1 mg/ml NHS-SS-biotin (Pierce Chemicals, Dallas, TX) for 20 min on ice. The reaction was quenched by washing three times with buffer (20 mM Tris and 120 mM NaCl, pH 7.4). After cell lysis, biotinylated proteins were bound to streptavidin-agarose beads (Pierce Chemicals), and precipitates were immunoblotted with mouse anti-HA (cl 11; Covance) to detect hERG. Densitometric analysis of hERG and its ubiquitination were performed using ImageJ 1.44p software (National Institutes of Health, Bethesda, MD) with background correction for each lane. Deglycosylation of wt hERG lysates with PNGase F and Endo H was performed as previously described (Akhavan et al., 2003; Glzman et al., 2009).

Limited proteolysis of hERG

Microsomes were prepared from hERG-expressing HeLa cells by nitrogen cavitation, followed by differential centrifugation, and were subjected to limited proteolysis, as described previously (Du et al., 2005). Briefly, microsomes were resuspended in either high-K⁺ (75 mM KCl, 10 mM HEPES, pH 7.4) or K⁺-free buffer (75 mM NMDG, 10 mM HEPES, pH 7.4) and digested with the indicated concentration of tosyl phenylalanyl chloromethyl ketone-treated trypsin (Worthington, Lakewood, NJ) or tosyllysine chloromethyl ketone-treated chymotrypsin (Sigma-Aldrich) for 10 min at 37°C. Where indicated, the luminal K⁺ concentration was clamped to 75 mM with 10 µM valinomycin and 10 µM CCCP.

Flame photometry

To determine the cellular K⁺ content, HeLa cells expressing wt-hERG were washed three times with K⁺-free NMDG buffer (150 mM NMDG, 20 mM HEPES, pH 7.4) and solubilized with K⁺-free lysis

buffer (1% Triton X-100, 150 mM NMDG, 25 mM Tris-HCl, pH 8.0) for 10 min on ice. Cellular debris was removed with centrifugation (15,000 × g, 10 min). The K⁺ content of cell lysates was determined by flame emission spectroscopic analysis (AAAnalyst 100; Perkin Elmer, Waltham, MA) and expressed as percentage of untreated cells. K⁺ content was normalized to protein concentration.

Immunostaining and confocal microscopy

HeLa cells expressing hERG were cultured on cover slips and fixed (4% paraformaldehyde in PBS, 15 min). Intracellular antigens were visualized on fixed, permeabilized (0.05% saponin) cells using the indicated primary Ab: mouse monoclonal anti-HA (1:1000; Covance), rabbit polyclonal anti-LAMP1 (1:1000; Abcam, Cambridge, MA), and polyclonal anti-early endosomal antigen 1 (EEA1; 1:1000; Affinity Bioreagents, Golden, CO). The postendocytic distribution of anti-HA labeled hERG (4°C for 60 min) was determined after the indicated chase in the absence of extracellular Ab before indirect immunostaining. Lysosomes were labeled either with Oregon 488- or Texas red-conjugated dextran (10 kDa, 50 µg/ml; Life Technologies) by overnight fluid-phase endocytosis and chased for >3 h at 37°C. Alexa 594-labeled transferrin uptake (10 µg/ml, 1 h at 37°C) was performed as described (Barriere et al., 2006). Alexa-labeled secondary antibodies were from Molecular Probes. Epifluorescence images were taken on a Zeiss Observer Z1 microscope (Carl Zeiss MicroImaging) equipped with an Evolve 512 electron-multiplying charge-coupled device (EM CCD) camera (Photometrics Technology, Tucson, AZ) and a 63×/1.4 numerical aperture (NA) Plan Apochromat oil-immersion objective. Confocal images were taken sequentially on a LSM710 microscope (Carl Zeiss MicroImaging) equipped with a Plan Apochromat 63×/NA 1.4 objective in multitrack mode. Single optical sections or epifluorescence images are shown. Image processing was performed with Photoshop CS3 (Adobe). Manders' correlation coefficient for colocalization of hERG with dextran (Figure 4) was calculated using ImageJ with JACOP plug-in.

Fluorescence ratio imaging analysis

The methodology for FRIA of endocytic vesicles is described in detail by Barriere and Lukacs (2008). Cargo labeling was accomplished by incubating the primary and secondary Abs sequentially on ice before internalization at 37°C or by loading the complex for 0.5–1 h. Mouse monoclonal anti-HA (1:1000; Covance) or concentrated ascites fluid against CD63/LAMP2 1:1 mixture (1:100, H5C6-c and H4B4; Developmental Studies Hybridoma Bank, University of Iowa, Iowa City, IA) were used with FITC-conjugated goat anti-mouse secondary Fab (Jackson ImmunoResearch). To monitor the fluid-phase marker, FITC-dextran (10 kDa, 50 µg/ml; Molecular Probes), lysosomal delivery, dextran was endocytosed for 1 h and chased for 2 h at 37°C. FRIA was performed on a Zeiss Observer Z1 inverted fluorescence microscope (Carl Zeiss MicroImaging) equipped with a X-Cite 120Q fluorescence illumination system (Lumen Dynamics Group, Canada) and Evolve 512 EM CCD camera (Photometrics Technology). The acquisition was carried out at 495 ± 5– and 440 ± 10-nm excitation wavelengths using a 535 ± 25-nm emission filter and analyzed with MetaFluor software (Molecular Devices, Canada).

Statistical analysis

Data are presented as mean ± SEM at least from three independent experiments. Statistical analysis was performed on Prism 5.0 or 6.0 (GraphPad). Significance was calculated at 95% confidence levels using one-tailed p values with unpaired t test.

ACKNOWLEDGMENTS

This work is dedicated to the memory of Eckhard Ficker, who passed away before submission of the manuscript. We thank Hung Lam for conducting pilot studies. We also thank the Canadian Institute of Health Research and the Canadian Foundation for Innovation for support. B.F. was recipient of Chemical Biology Training Program and GRASP fellowships. G.L. is the holder of a Canada Research Chair.

REFERENCES

- Akhavan A, Atanasiu R, Shrier A (2003). Identification of a COOH-terminal segment involved in maturation and stability of human ether-a-go-go-related gene potassium channels. *J Biol Chem* 278, 40105–40112.
- Albesa M, Grilo LS, Gavillet B, Abriel H (2011). Nedd4-2-dependent ubiquitylation and regulation of the cardiac potassium channel hERG1. *J Mol Cell Cardiol* 51, 90–98.
- Anderson CL, Delisle BP, Anson BD, Kilby JA, Will ML, Tester DJ, Gong Q, Zhou Z, Ackerman MJ, January CT (2006). Most LQT2 mutations reduce Kv11.1 (hERG) current by a class 2 (trafficking-deficient) mechanism. *Circulation* 113, 365–373.
- Apaja PM, Xu H, Lukacs GL (2010). Quality control for unfolded proteins at the plasma membrane. *J Cell Biol* 191, 553–570.
- Arvan P, Zhao X, Ramos-Castaneda J, Chang A (2002). Secretory pathway quality control operating in Golgi, plasmalemmal, and endosomal systems. *Traffic* 3, 771–780.
- Barriere H, Apaja P, Okiyone T, Lukacs GL (2011). Endocytic sorting of CFTR variants monitored by single-cell fluorescence ratiometric image analysis (FRIA) in living cells. *Methods Mol Biol* 741, 301–317.
- Barriere H, Lukacs GL (2008). Analysis of endocytic trafficking by single-cell fluorescence ratio imaging. *Curr Protoc Cell Biol Chapter* 15, Unit 15.13.
- Barriere H, Nemes C, Lechardeur D, Khan-Mohammad M, Fruh K, Lukacs GL (2006). Molecular basis of oligoubiquitin-dependent internalization of membrane proteins in Mammalian cells. *Traffic* 7, 282–297.
- Beller GA, Smith TW, Abelmann WH, Haber E, Hood WB Jr (1971). Digitalis intoxication. A prospective clinical study with serum level correlations. *N Engl J Med* 284, 989–997.
- Boehmer C, Laufer J, Jeyaraj S, Klaus F, Lindner R, Lang F, Palmada M (2008). Modulation of the voltage-gated potassium channel Kv1.5 by the SGK1 protein kinase involves inhibition of channel ubiquitination. *Cell Physiol Biochem* 22, 591–600.
- Boname JM, Thomas M, Stagg HR, Xu P, Peng J, Lehner PJ (2010). Efficient internalization of MHC I requires lysine-11 and lysine-63 mixed linkage polyubiquitin chains. *Traffic* 11, 210–220.
- Brodsky JL, Skach WR (2011). Protein folding and quality control in the endoplasmic reticulum: Recent lessons from yeast and mammalian cell systems. *Curr Opin Cell Biol* 23, 464–475.
- Ciechanover A, Gropper R, Schwartz AL (1991). The ubiquitin-activating enzyme is required for lysosomal degradation of cellular proteins under stress. *Biomed Biochim Acta* 50, 321–332.
- Connell P, Ballinger CA, Jiang J, Wu Y, Thompson LJ, Hohfeld J, Patterson C (2001). The co-chaperone CHIP regulates protein triage decisions mediated by heat-shock proteins. *Nat Cell Biol* 3, 93–96.
- Cordes JS, Sun Z, Lloyd DB, Bradley JA, Opsahl AC, Tengowski MW, Chen X, Zhou J (2005). Pentamidine reduces hERG expression to prolong the QT interval. *Br J Pharmacol* 145, 15–23.
- Cyr DM, Hohfeld J, Patterson C (2002). Protein quality control: U-box-containing E3 ubiquitin ligases join the fold. *Trends Biochem Sci* 27, 368–375.
- Delisle BP, Anderson CL, Balijepalli RC, Anson BD, Kamp TJ, January CT (2003). Thapsigargin selectively rescues the trafficking defective LQT2 channels G601S and F805C. *J Biol Chem* 278, 35749–35754.
- Dennis AT, Nassal D, Deschenes I, Thomas D, Ficker E (2011). Antidepressant-induced ubiquitination and degradation of the cardiac potassium channel hERG. *J Biol Chem* 286, 34413–34425.
- Dennis A, Wang L, Wan X, Ficker E (2007). hERG channel trafficking: novel targets in drug-induced long QT syndrome. *Biochem Soc Trans* 35, 1060–1063.
- Dennis AT, Wang L, Wan H, Nassal D, Deschenes I, Ficker E (2012). Molecular determinants of pentamidine-induced hERG trafficking inhibition. *Mol Pharmacol* 81, 198–209.
- Du K, Sharma M, Lukacs GL (2005). The DeltaF508 cystic fibrosis mutation impairs domain-domain interactions and arrests post-translational folding of CFTR. *Nat Struct Mol Biol* 12, 17–25.
- Duarri A et al. (2008). Molecular pathogenesis of megalencephalic leukoencephalopathy with subcortical cysts: mutations in MLC1 cause folding defects. *Hum Mol Genet* 17, 3728–3739.
- Ficker E, Dennis AT, Wang L, Brown AM (2003). Role of the cytosolic chaperones Hsp70 and Hsp90 in maturation of the cardiac potassium channel hERG. *Circ Res* 92, e87–e100.
- Ficker E, Kurshev YA, Dennis AT, Obejero-Paz C, Wang L, Hawryluk P, Wible BA, Brown AM (2004). Mechanisms of arsenic-induced prolongation of cardiac repolarization. *Mol Pharmacol* 66, 33–44.
- Furutani M et al. (1999). Novel mechanism associated with an inherited cardiac arrhythmia: defective protein trafficking by the mutant HERG (G601S) potassium channel. *Circulation* 99, 2290–2294.
- Gheorghie M, Lukas MA (2004). Role of carvedilol in atrial fibrillation: insights from clinical trials. *Am J Cardiol* 93, 53B–57B.
- Glozman R, Okiyone T, Mulvihill CM, Rini JM, Barriere H, Lukacs GL (2009). N-glycans are direct determinants of CFTR folding and stability in secretory and endocytic membrane traffic. *J Cell Biol* 184, 847–862.
- Guo J, Massaeli H, Li W, Xu J, Luo T, Shaw J, Kirshenbaum LA, Zhang S (2007). Identification of IKr and its trafficking disruption induced by probufol in cultured neonatal rat cardiomyocytes. *J Pharmacol Exp Ther* 321, 911–920.
- Guo J, Massaeli H, Xu J, Jia Z, Wigle JT, Mesaeli N, Zhang S (2009). Extracellular K⁺ concentration controls cell surface density of IKr in rabbit hearts and of the HERG channel in human cell lines. *J Clin Invest* 119, 2745–2757.
- Gustina AS, Trudeau MC (2013). The eag domain regulates hERG channel inactivation gating via a direct interaction. *J Gen Physiol* 141, 229–241.
- Haardt M, Benharouga M, Lechardeur D, Kartner N, Lukacs GL (1999). C-terminal truncations destabilize the cystic fibrosis transmembrane conductance regulator without impairing its biogenesis. A novel class of mutation. *J Biol Chem* 274, 21873–21877.
- Henne WM, Buchkovich NJ, Emr SD (2011). The ESCRT pathway. *Dev Cell* 21, 77–91.
- Harley CA, Jesus CS, Carvalho R, Brito RM, Morais-Cabral JH (2012). Changes in channel trafficking and protein stability caused by LQT2 mutations in the PAS domain of the HERG channel. *PLoS One* 7, e32654.
- Hauptman PJ, Kelly RA (1999). Digitalis. *Circulation* 99, 1265–1270.
- Hawryluk MJ, Keyel PA, Mishra SK, Watkins SC, Heuser JE, Traub LM (2006). Epsin 1 is a polyubiquitin-selective clathrin-associated sorting protein. *Traffic* 7, 262–281.
- Henke G, Maier G, Wallisch S, Boehmer C, Lang F (2004). Regulation of the voltage gated K⁺ channel Kv1.3 by the ubiquitin ligase Nedd4-2 and the serum and glucocorticoid inducible kinase SGK1. *J Cell Physiol* 199, 194–199.
- Keating MT, Sanguinetti MC (2001). Molecular and cellular mechanisms of cardiac arrhythmias. *Cell* 104, 569–580.
- Keener JM, Babst M (2013). Quality control and substrate-dependent downregulation of the nutrient transporter Fur4. *Traffic* 14, 412–427.
- Ke Y, Ng CA, Hunter MJ, Mann SA, Heide J, Hill AP, Vandenberg JI (2013). Trafficking defects in PAS domain mutant Kv1.1 channels: roles of reduced domain stability and altered domain-domain interactions. *Biochem J* 454, 69–77.
- Kim HT, Kim KP, Lledias F, Kisselev AF, Scaglione KM, Skowyra D, Gygi SP, Goldberg AL (2007). Certain pairs of ubiquitin-conjugating enzymes (E2s) and ubiquitin-protein ligases (E3s) synthesize nondegradable forked ubiquitin chains containing all possible isopeptide linkages. *J Biol Chem* 282, 17375–17386.
- Krishnan MN, Bingham JP, Lee SH, Trombley P, Moczydlowski E (2005). Functional role and affinity of inorganic cations in stabilizing the tetrameric structure of the KcsA K⁺ channel. *J Gen Physiol* 126, 271–283.
- Kuryshov YA et al. (2005). Pentamidine-induced long QT syndrome and block of hERG trafficking. *J Pharmacol Exp Ther* 312, 316–323.
- Lamothe SM, Zhang S (2013). The serum- and glucocorticoid-inducible kinases SGK1 and SGK3 regulate hERG channel expression via ubiquitin ligase Nedd4-2 and GTPase Rab11. *J Biol Chem* 288, 15075–15084.
- Lockless SW, Zhou M, MacKinnon R (2007). Structural and thermodynamic properties of selective ion binding in a K⁺ channel. *PLoS Biol* 5, e121.
- MacGurn JA, Hsu PC, Emr SD (2012). Ubiquitin and membrane protein turnover: from cradle to grave. *Annu Rev Biochem* 81, 231–259.
- Maier G, Palmada M, Rajamanickam J, Shumilina E, Bohmer C, Lang F (2006). Upregulation of HERG channels by the serum and glucocorticoid inducible kinase isoform SGK3. *Cell Physiol Biochem* 18, 177–186.
- Massaeli H, Guo J, Xu J, Zhang S (2010a). Extracellular K⁺ is a prerequisite for the function and plasma membrane stability of HERG channels. *Circ Res* 106, 1072–1082.

- Massaeli H, Sun T, Li X, Shallow H, Wu J, Xu J, Li W, Hanson C, Guo J, Zhang S (2010b). Involvement of caveolin in low K⁺-induced endocytic degradation of cell-surface human ether-a-go-go-related gene (hERG) channels. *J Biol Chem* 285, 27259–27264.
- Meacham GC, Patterson C, Zhang W, Younger JM, Cyr DM (2001). The Hsc70 co-chaperone CHIP targets immature CFTR for proteasomal degradation. *Nat Cell Biol* 3, 100–105.
- Okiyoneda T, Apaja PM, Lukacs GL (2011). Protein quality control at the plasma membrane. *Curr Opin Cell Biol* 23, 483–491.
- Okiyoneda T, Barriere H, Bagdany M, Rabeh WM, Du K, Hohfeld J, Young JC, Lukacs GL (2010). Peripheral protein quality control removes unfolded CFTR from the plasma membrane. *Science* 329, 805–810.
- Rajamani S et al. (2006). Drug-induced long QT syndrome: hERG K⁺ channel block and disruption of protein trafficking by fluoxetine and norfluoxetine. *Br J Pharmacol* 149, 481–489.
- Ren X, Hurley JH (2010). VHS domains of ESCRT-0 cooperate in high-avidity binding to polyubiquitinated cargo. *EMBO J* 29, 1045–1054.
- Sanguinetti MC, Jiang C, Curran ME, Keating MT (1995). A mechanistic link between an inherited and an acquired cardiac arrhythmia: HERG encodes the IKr potassium channel. *Cell* 81, 299–307.
- Sanguinetti MC, Tristani-Firouzi M (2006). hERG potassium channels and cardiac arrhythmia. *Nature* 440, 463–469.
- Sharma M et al. (2004). Misfolding diverts CFTR from recycling to degradation: quality control at early endosomes. *J Cell Biol* 164, 923–933.
- Sun T et al. (2011). The role of monoubiquitination in endocytic degradation of human ether-a-go-go-related gene (hERG) channels under low K⁺ conditions. *J Biol Chem* 286, 6751–6759.
- Takemasa H et al. (2008). Coexistence of hERG current block and disruption of protein trafficking in ketoconazole-induced long QT syndrome. *Br J Pharmacol* 153, 439–447.
- Vandenberg JI, Perry MD, Perrin MJ, Mann SA, Ke Y, Hill AP (2012). hERG K(+) channels: structure, function, and clinical significance. *Physiol Rev* 92, 1393–1478.
- Walker VE, Atanasiu R, Lam H, Shrier A (2007). Co-chaperone FKBP38 promotes HERG trafficking. *J Biol Chem* 282, 23509–23516.
- Walker VE, Wong MJ, Atanasiu R, Hantouche C, Young JC, Shrier A (2010). Hsp40 chaperones promote degradation of the HERG potassium channel. *J Biol Chem* 285, 3319–3329.
- Wang DT, Hill AP, Mann SA, Tan PS, Vandenberg JI (2011). Mapping the sequence of conformational changes underlying selectivity filter gating in the Kv11.1 potassium channel. *Nat Struct Mol Biol* 18, 35–41.
- Wang L, Dennis AT, Trieu P, Charron F, Ethier N, Hebert TE, Wan X, Ficker E (2009). Intracellular potassium stabilizes human ether-a-go-go-related gene channels for export from endoplasmic reticulum. *Mol Pharmacol* 75, 927–937.
- Wang L, Wible BA, Wan X, Ficker E (2007). Cardiac glycosides as novel inhibitors of human ether-a-go-go-related gene channel trafficking. *J Pharmacol Exp Ther* 320, 525–534.
- Wible BA, Hawryluk P, Ficker E, Kuryshov YA, Kirsch G, Brown AM (2005). HERG-Lite: a novel comprehensive high-throughput screen for drug-induced hERG risk. *J Pharmacol Toxicol Methods* 52, 136–145.
- Zhou Y, MacKinnon R (2003). The occupancy of ions in the K⁺ selectivity filter: charge balance and coupling of ion binding to a protein conformational change underlie high conduction rates. *J Mol Biol* 333, 965–975.